U.S. DEPARTMENT OF COMMERCE
NATIONAL OCEANIC AND ATMOSPHERIC ADMINISTRATION
NATIONAL WEATHER SERVICE
NATIONAL METEOROLOGICAL CENTER

OFFICE NOTE 166

Linear Analysis of a Simplified Semi-Implicit Model with Some Ideas Given Regarding Geostrophic Adjustment, Small Grid Length Modeling, and Vertical Resolution

William G. Collins
Development Division

JANUARY 1978

Linear Analysis of a Simplified Semi-implicit Model with Some Ideas Given Regarding Geostrophic Adjustment, Small Grid Length Modeling, and Vertical Resolution.

1. Introduction

Various approximations have been used in numerical weather prediction models to allow the maximum useful time step, with economy being the guiding force. Among the approximations used are: the hydrostatic approximation--removing acoustic waves, the quasi-geostrophic approximation--removing gravity waves, and semi-implicit time differencing--slowing down the phase speeds of gravity waves. In all cases it has been argued that the motions that were removed or whose accuracy was affected, were not essential to the meteorologically important fields.

This note will consider some of the effects of the semi-implicit time differencing. This method amounts to a time averaging of terms in the equations of motion that are responsible for gravity wave motion, thereby slowing them down. As a result, a longer time step may be used. This note will concentrate on the limitations of this method, particularly for high-resolution models.

Office Note 155 gave the equations for a semi-implicit slab model. The model was used there to test certain solution algorithms, and it will be used in the future to check some of the conclusions of this note by actual numerical calculation. In this note the equations are linearized and the phase speeds of the waves are examined as a function of the time step, the horizontal scale, and the vertical structure. Comparisons are made between the analytic phase speeds and group velocities and the phase speeds and group velocities calculated by various time differencing.

2. Linear analysis of the semi-implicit model

The reader is referred to Office Note 155 for the model equations in finite-difference form. Only their linear counterpart will be given here. They are

$$\overline{u}_k^{2t} = u_k^{\tau-1} + \Delta t\ f\ \overline{v}_k^{yy^\tau} \tag{1}$$

$$\overline{v}_k^{2t} + \tfrac{1}{2}\Delta t\left(\overline{\phi}_k^{2t} + \overline{\phi}_{k+1_y}^{2t}\right) = v_k^{\tau-1} - \Delta t\ f\ \overline{u}_k^{yy^\tau} \tag{2}$$

$$\overline{\theta}_k^{2t} + \tfrac{1}{2}\Delta t\ \overline{\theta}_{k_p}\left(\overline{\omega}_k^{2t} + \overline{\omega}_{k+1}^{2t}\right) = \theta'^{\tau-1}_k \tag{3}$$

$$\overline{\phi}'^{2t}_{k+1} - \overline{\phi}'^{2t}_k + c_p\Delta\pi_k\overline{\theta}'^{2t}_k = 0 \tag{4}$$

$$\overline{\phi}_1^{2t} - \Delta t\ \alpha_s\overline{\omega}_1^{2t} = \phi_1^{\tau-1} \tag{5}$$

$$\Delta p_k \, \overline{v_{ky}}^{2t} + \overline{\omega_{k+1}}^{2t} - \overline{\omega_k}^{2t} = 0 \tag{6}$$

$$\omega_{L+1} = 0 \tag{7}$$

where u is the west wind speed; v is the south wind speed; θ' is the deviation of potential temperature from the mean; ϕ' is the deviation of the geopotential from the mean; ω is the total derivative of pressure with respect to time; α_s is the surface value of the specific volume; k is an index for the model layer and all other variables have their usual meanings. Fig. 1 shows the arrangement of model variables in space. L is the number of layers. And $\overline{\theta}_{k_p} = d\theta_k/dp$. Also,

$$\overline{(\;)}^{2t} = \tfrac{1}{2}[(\;)^{\tau+1} + (\;)^{\tau-1}] \tag{8}$$

The vertical variation of variables is separated from the horizontal and time variation by introducing

$$\begin{pmatrix} u_k \\ v_k \\ \theta'_k \\ \phi'_k \\ \omega_k \end{pmatrix} = \begin{pmatrix} \hat{u}_k \\ \hat{v}_k \\ \hat{\theta}_k \\ \hat{\phi}_k \\ \hat{\omega}_k \end{pmatrix} \exp[i(\ell m\Delta y + \sigma n\Delta t)] \tag{9}$$

It is noted that

$$\begin{aligned} \overline{(\;)}^{2t} &= \cos(\sigma\Delta t)\ \exp[\;] \\ \overline{(\;)}^{2t} - (\;)^{\tau-1} &= i \sin(\sigma\Delta t)\ \exp[\;] \\ \overline{(\;)}^{yy} &= \cos^2\left(\frac{\ell\Delta y}{2}\right) \exp[\;] \end{aligned} \tag{10}$$

Introduce (9), use (10), and make the following definitions:

$$\begin{aligned} S &\equiv \sin(\sigma\Delta t) \\ C &\equiv \cos(\sigma\Delta t) \\ \ell^* &\equiv \ell\,\frac{\sin\ell\Delta y}{\ell\Delta y} \\ A^* &= \cos^2\left(\frac{\ell\Delta y}{2}\right) \end{aligned} \tag{11}$$

Then (1)-(6) become

$$iS\ \hat{u}_k - A^*f\Delta t\ \hat{v}_k = 0 \tag{12}$$

$$iS\ \hat{v}_k + \tfrac{1}{2}\, i\ \ell^*\Delta t C(\hat{\phi}_k + \hat{\phi}_{k+1}) + A^*f\Delta t\ \hat{u}_k = 0 \tag{13}$$

$$iS\ \hat{\theta}_k + \tfrac{1}{2}\ \Delta t\ C\overline{\theta}_{k_p}(\hat{\omega}_k + \hat{\omega}_{k+1}) = 0 \tag{14}$$

$$\hat{\phi}_{k+1} - \hat{\phi}_k + c_p\ \Delta\ \pi_k\ \hat{\theta}_k = 0 \tag{15}$$

$$iS\hat{\phi}_1 - \Delta t\ \alpha_s\ C\ \hat{\omega}_1 = 0 \tag{16}$$

$$i\ell^*\ \Delta p_k\ \hat{v}_k + \hat{\omega}_{k+1} - \hat{\omega}_k = 0 \tag{17}$$

We further define

$$\overline{\phi}_k \equiv \hat{\phi}_k + \hat{\phi}_{k+1} \tag{18}$$

The set of equations, (12)-(17) and (7) can be reduced to a set of L equations in the L unknowns $\overline{\phi}_1, \overline{\phi}_2, \ldots, \overline{\phi}_L$. That set of equations is

$$[C_*^2 - C_k^2 + (-1)^k\ \gamma_k^2]\overline{\phi}_k + 2(-1)^k \sum_{j=1}^{k-1}[\tfrac{1}{2}\gamma_j^2 + (-1)^j\ C_*^2]\overline{\phi}_j$$

$$+ \sum_{j=k+1}^{L}[(-1)^k\gamma_j^2 - 2C_k^2\ r_{jk}]\overline{\phi}_j = 0\ , \quad k = 1,2,\ldots,L \tag{19}$$

where

$$C_*^2 = \frac{S^2 - f^2\Delta t^2 A^{*2}}{C^2\ell^{*2}\Delta t^2} \tag{20}$$

$$C_k^2 = -\tfrac{1}{4}\ c_p\Delta\pi_k\overline{\theta}_{k_p}\Delta p_k \tag{21}$$

$$\gamma_k^2 = -\ \alpha_s\Delta p_k \tag{22}$$

$$r_{jk} = \frac{\Delta p_j}{\Delta p_k} \tag{23}$$

Equation (19) can be written conveniently in matrix form as

$$A\Phi = 0 \tag{24}$$

where

$$\Phi^T = \left(\overline{\Phi}_1, \overline{\Phi}_2, \ldots, \overline{\Phi}_L\right) \quad \left(\Phi^T \text{ is } \Phi \text{ transpose}\right)$$

and

$$A = \begin{pmatrix} \left(C_*^2 - C_1 - \gamma_1^2\right) & \left(-\gamma_2^2 - 2C_1^2 r_{21}\right) & \left(-\gamma_3^2 - 2C_1^2 r_{31}\right) & \left(-\gamma_4^2 - 2C_1^2 r_{41}\right) & \cdots & \left(-\gamma_L^2 - 2C_1^2 r_{L1}\right) \\ 2\left(\tfrac{1}{2}\gamma_1^2 - C_*^2\right) & \left(C_*^2 - C_2^2 + \gamma_2^2\right) & \left(\gamma_3^2 - 2C_2^2 r_{32}\right) & \left(\gamma_4^2 - 2C_2^2 r_{42}\right) & \cdots & \left(\gamma_L^2 - 2C_2^2 r_{L2}\right) \\ -2\left(\tfrac{1}{2}\gamma_1^2 - C_*^2\right) & -2\left(\tfrac{1}{2}\gamma_2^2 + C_*^2\right) & \left(C_*^2 - C_3^2 - \gamma_3^2\right) & \left(-\gamma_4^2 - 2C_3^2 r_{43}\right) & \cdots & \left(-\gamma_L - 2C_3^2 r_{L3}\right) \\ 2\left(\tfrac{1}{2}\gamma_1^2 - C_*^2\right) & 2\left(\tfrac{1}{2}\gamma_2^2 + C_*^2\right) & 2\left(\tfrac{1}{2}\gamma_3^2 - C_*^2\right) & \left(C_*^2 - C_4^2 + \gamma_4^2\right) & \cdots & \left(\gamma_L^2 - 2C_4^2 r_{L4}\right) \\ \vdots & \vdots & \vdots & \vdots & & \vdots \\ 2(-1)^L\left(\tfrac{1}{2}\gamma_1^2 - C_*^2\right) & 2(-1)^L\left(\tfrac{1}{2}\gamma_2^2 + C_*^2\right) & 2(-1)^L\left(\tfrac{1}{2}\gamma_3^2 - C_*^2\right) & 2(-1)^L\left(\tfrac{1}{2}\gamma_4^2 + C_*^2\right) & \cdots & \left(C_*^2 - C_L^2 + (-1)^L \gamma_L^2\right) \end{pmatrix} \tag{25}$$

In (25), C_* is the phase speed of gravity waves on a non-rotating earth. According to (20) and (11)

$$c_*^2 = \frac{\sin^2(\sigma\Delta t) - f^2\Delta t^2 \cos^2\left(\frac{\ell\Delta y}{2}\right)}{\ell^2\Delta t^2 \cos^2(\sigma\Delta t)\, \frac{\sin^2 \ell\Delta y}{\ell^2\Delta y^2}} \tag{26}$$

From this equation, we may solve for $\sigma\Delta t$.

$$\sigma\Delta t = \cos^{-1}\left(\left(\frac{1 - f^2\Delta t^2\cos^2\left(\frac{\ell\Delta y}{2}\right)}{1 + C_*^2\, \ell^2\Delta t^2 \frac{\sin^2 \ell\Delta y}{\ell^2\Delta y^2}}\right)^{\frac{1}{2}}\right) \tag{27}$$

From this we infer that σ will be real if the argument of the cosine inverse is between -1 and +1. Since

$$C_*^2 \ell^2\Delta t^2 \frac{\sin^2 \ell\Delta y}{\ell^2\Delta y^2} \geq 0 \ ,$$

this will be true for

$$0 \leq f^2\Delta t^2\cos^2\left(\frac{\ell\Delta y}{2}\right) \leq 1 \tag{28}$$

This is the stability criterion for this model.

It can be shown that if (28) is satisfied, the C_* is real. Suppose (28) is satisfied. Then, from (27)

$$1 \geq \left(1 + C_*^2\,\ell^2\Delta t^2\frac{\sin^2\ell\Delta y}{\ell^2\Delta y^2}\right)\cos^2(\sigma\Delta t) \geq 0$$

or

$$1 \geq 1 + C_*^2\,\ell^2\,\Delta t^2\,\frac{\sin^2\ell\Delta y}{\ell^2\Delta y^2} \geq 0$$

or

$$0 \leq C_*^2\,\ell^2\Delta t^2\,\frac{\sin^2\ell\Delta y}{\ell^2\Delta y^2} \leq 1\ .$$

Using (26)

$$0 \leq C_*^2\,\ell^2\Delta t^2\,\frac{\sin^2\ell\Delta y}{\ell^2\Delta y^2} = \frac{\sin^2(\sigma\Delta t) - f^2\Delta t^2\cos^2\left(\frac{\ell\Delta y}{2}\right)}{\cos^2(\sigma\Delta t)} \leq 1 \tag{29}$$

and therefore $C_*^2 \geq 0$, implying that C_* is real.

The values of C_*^2 which satisfy (24) are called eigenvalues of A. In all cases of interest, there will be one real value of C_*^2 for each model layer. The values will depend upon the basic state temperatures and upon f, ℓ, Δy, and Δt.

The values of C_* in specific cases of interest will be given later, but now let's consider (27) in much fuller detail, assuming that the values of C_*^2 are known. Note that (27) can be put in non-dimensional form by letting

$$\begin{aligned} \Omega_c &= \sigma\Delta t \\ F_*^{\,2} &= f^2\Delta t^2\cos^2(\ell\Delta y/2) \\ \Gamma_*^{\,2} &= C_*^{\,2}\ell^2\Delta t^2\left(\frac{\sin\ell\Delta y}{\ell\Delta y}\right)^2 \end{aligned} \tag{30}$$

The result is

$$\Omega_c = \cos^{-1}\left(\left(\frac{1-F_*^{\,2}}{1+\Gamma_*^{\,2}}\right)^{\frac{1}{2}}\right) = \tan^{-1}\left(\left(\frac{\Gamma_*^{\,2}+F_*^{\,2}}{1 - F_*^{\,2}}\right)^{\frac{1}{2}}\right) \tag{31}$$

Ω_c represents the angular displacement (in radians) of a wave in one time step. On the other hand, the analytic angular displacement, Ω_a, is

$$\Omega_a = (\Gamma^2 + F^2)^{\frac{1}{2}} \tag{32}$$

where

$$\begin{aligned} \Gamma^2 &= C_*^2 \ell^2 \Delta t^2 \\ F^2 &= f^2 \Delta t^2 \end{aligned} \tag{33}$$

This relationship can be seen from (26) by letting $\Delta t, \Delta y \to 0$. Figure 2 shows Ωa. Figure 3 shows Ωc. And Figure 4a-4d shows $\Omega c/\Omega a$. In several of these and succeeding figures, dashed lines will be shown. They are lines along which Γ/F or Γ_*/F_* is constant. Moving along one of these lines shows the effect of changing Δt only. In Figure 4a, horizontal differencing is disregarded so that $\Gamma=\Gamma_*$ and $F=F_*$, while in Figures 4b-4d the difference between Γ and Γ_* and between F and F_* is taken into account. An additional parameter is introduced by the horizontal differencing, namely $\Delta y/\lambda$, where λ, the "radius of deformation" is defined by

$$\lambda = \frac{C_*}{f} \quad .$$

The radius of deformation is related to the size of the circle of a particle in pure inertial motion. Therefore, $\Delta y/\lambda = 1/32$ represents a good resolution of inertial motions. $\Delta y/\lambda = \frac{1}{4}$ represents moderate resolution, and $\Delta y/\lambda = 1$ represents poor resolution of inertial motions. In Figures 4b-4d the value of $\Delta y/\lambda$ is 1/32, 1/4 and 1, respectively. Almost all discussions will be in terms of 4a, which can be considered to be the limit of $\Delta y/\lambda \to 0$, but the reader can make other comparisons as desired.

Let's consider Figures 2-4 in detail. Figure 2 gives the angular displacement, of a wave with a particular C_*^2, in one time step. Since the analytic phase speed does not depend upon Δt, the displacement is merely proportional to Δt. This may be seen by following any dashed line in Figure 2. We may delineate three regions in the Γ-F plane. For $\Gamma/F \geq 2$ it is found that Ω is roughly proportional to Γ, i.e., to ℓC_*. Waves in this region are predominantly gravity waves. On the other hand, within the region where $\Gamma/F \leq 1/3$, it is found that Ω is nearly independent of Γ. These waves are predominantly inertial waves. Between these regions are waves of mixed form.

In order to give a concrete basis to this classification, Table 1 has been formed which lists values of $R=\Gamma/F$ for typical scales of atmospheric motions. The table also lists the implied predominant wave form.

Table 1

Low latitudes: $f = 0.3 \times 10^{-4} s^{-1}$

	external wave $c_* = 350\ ms^{-1}$	internal wave $c_* = 100\ ms^{-1}$
Mesoscale: $\ell \simeq 10^{-5}\ m^{-1}$	R = 117 gravity	R = 33 gravity
Synoptic scale: $\ell \simeq 10^{-6}\ m^{-1}$	R = 11.7 gravity	R = 3.3 gravity
Global scale: $\ell \simeq 3 \times 10^{-7}\ m^{-1}$	R = 3.5 gravity	R = 1.0 mixed

High latitudes: $f = 1.2 \times 10^{-4} s^{-1}$

	external wave $c_* = 350\ ms^{-1}$	internal wave $c_* = 100\ ms^{-1}$
Mesoscale: $\ell \simeq 10^{-5}\ m^{-1}$	R = 29.2 gravity	R = 8.3 gravity
Synoptic scale: $\ell \simeq 10^{-6}\ m^{-1}$	R = 2.9 gravity	R = .8 mixed
Global scale: $\ell \simeq 3 \times 10^{-7}\ m^{-1}$	R = .9 mixed	R = .25 inertial

It is pointed out that the conclusions of Table 1 are severely limited on the global scale, since the variation of the Coriolis parameter has not been included in this analysis.

Figure 3 shows the computed angular displacement per timestep for the semi-implicit modes. For $F_* \leq 0.5$ and for $\Gamma/F \leq 1/3$, the displacements compare very favorably with the analytic displacements. The errors in this region are less than 5%. Outside this region, two factors lead to error. First, for $F_* \to 1.0$, all displacements approach $\pi/2$. This is connected with the stability criterion. And secondly, for Γ_* greater than about 1.0, the semi-implicit differencing greatly slows down the waves. These waves are seen to be predominantly gravity waves. Since one of the usual objectives of the semi-implicit formulation is to slow down gravity waves so that they can be stably calculated with a longer time step, this objective is met. It would be desirable to limit F_* to less than .5, however, so that the inertial waves are calculated accurately.

Figure 4 emphasizes these points by giving the ratio $\Omega c/\Omega a$. By following a dashed line we may see the effect of varying the time step, with all other parameters fixed.

Figure 5 shows the calculated angular displacement for a model that is identical to the semi-implicit model except that centered (leapfrog) time differencing is used. Figure 5a-6d shows the ratio $\Omega E/\Omega a$ for various values of $\Delta y/\lambda$. Figure 6a gives the limit for small $\Delta y/\lambda$. It is this figure that will be primarily discussed.

It is seen that the explicit model generally calculates phase speeds in excess of the analytic phase speed. The only exceptions are waves of relatively few grid lengths in size. This can be seen in Figures 6b-6d. For $\Gamma_*^2 + F_*^2 < \frac{1}{2}$, the explicit model errors are generally quite small. There is no distinction in the time-differencing effect between inertial and gravity waves. Comparison with Figure 4 shows that, even within the region $\Gamma_*^2+F_*^2 < \frac{1}{2}$, the semi-implicit time differencing selectively damps the gravity waves. Both methods have nearly the same effect upon the inertial waves. Since the inertial waves are treated explicitly by the semi-implicit model, this is to be expected. A reduction of time-step for the explicit model uniformly increases the accuracy of the gravity wave and inertial wave phase speeds, except for the shortest waves for which the space differencing error is overwhelming.

3. Group velocities

Not only are phase velocities important for the accurate calculation of meteorological fields, but group velocities are also, for energy is propagated at the group velocity speed. For the problem of geostrophic adjustment, the adjustment cannot progress at a greater speed than the group velocity of the waves participating in the adjustment.

The following equations give the analytic group velocity, the group velocity for the semi-implicit model, and the group velocity for a corresponding explicit model. The model group velocities include the effect of spacial differencing.

<u>analytic</u>

$$\frac{d\sigma_a}{d\ell} = \frac{\Gamma C_*}{(\Gamma^2 + F^2)^{\frac{1}{2}}} = \frac{(\Gamma/F)C_*}{[(\Gamma/F)^2 + 1)]^{\frac{1}{2}}} \tag{34}$$

semi-implicit

$$\frac{d\sigma_c}{d\ell} = \frac{\Gamma_* C_*}{(\Gamma_*^2 + F_*^2)^{\frac{1}{2}}}[1 - \Gamma_*^2 - F_*^2]^{-\frac{1}{2}}[\cos\ell\Delta y - \left(\frac{\Delta y}{2\lambda}\right)^2] \tag{35}$$

explicit (leapfrog)

$$\frac{d\sigma_E}{d\ell} = \frac{\Gamma_* C_*}{(\Gamma_*^2 + F_*^2)^{\frac{1}{2}}} \frac{(1 - F_*^2)^{\frac{1}{2}}}{1 + \Gamma_*^2}[\cos\ell\Delta y - \frac{1 + \Gamma_*^2}{1 - F_*^2}\left(\frac{\Delta y}{2\lambda}\right)^2] \tag{36}$$

The analytic group velocity depends only upon two parameters, e.g., (Γ/F) and C_*. The semi-implicit and explicit group velocities, on the other hand, depend upon four parameters, which may be taken to be F_*, Γ_*, $\Delta y/\lambda$, and C_*. $\ell\Delta y$ is not an additional independent parameter since

$$\ell\Delta y = 2\sin^{-1}\left(\tfrac{1}{2}\frac{\Delta y}{\lambda}\frac{\Gamma_*}{F_*}\right), \text{ where } \lambda = \frac{C_*}{f} = \frac{\Gamma}{\ell F} \tag{37}$$

The errors of the model group velocities are rather complex. Figures will be given which show the ratio of the model group velocity to the analytic group velocity for three values of $\Delta y/\lambda$, namely 1/32, 1/4, and 1.

First, the analytic group velocity, relative to C_* is given in Figure 7. It is only a function of Γ/F as expressed by eqn. (34). For gravity waves, $d\sigma/d\ell \geq .9C_*$. For mixed waves $.32C_* \leq d\sigma/d\ell \leq .9C_*$. And for inertial waves $d\sigma/d\ell \leq .32C_*$.

Figures 8a to 8c show the semi-implicit model group velocities divided by the analytic group velocities, for $\Delta y/\lambda$ = 1/32, 1/4, and 1. First, notice the changes for each model as $\Delta y/\lambda$ increases. For both models, the largest changes are to the gravity waves. Indeed, for $\Delta y/\lambda = 1$, any gravity waves are near two grid increments in wavelength. Both models have large negative group velocities for these waves. In general, waves between 2 and 4 grid lengths long have negative group velocities. Further, both models have very large (+ or -) group velocities near the model stability limits.

There are some basic differences between the two model group velocities. The semi-implicit group velocity decreases as F_* increases (except for very small F_*) while the explicit model group velocity increases as F_* increases (except for very small F_*). The same was shown earlier to be true of the model phase velocities. Other comparisons are left to the reader.

4. Applications

The following paragraphs will consider some applications of the semi-implicit model analysis:

a. Small grid length models

Smaller and smaller grid lengths are used in numerical models in order to reduce the truncation error. The objectives are at least two-fold: (1) to reduce the error in calculation of a feature with given wavelength, and (2) to be able to include smaller and smaller features with reasonable accuracy. These objectives will be considered one at a time.

First will be considered the phase speed error reduction as Δy is reduced while Δt is fixed. Figure 4 shows $\Omega c/\Omega a$. As Δy is reduced, F_* will be reduced as given by $F_* = f\Delta t \cos \ell\Delta y/2$. The reduction to Γ_* will be nearly the same since

$$\frac{\Gamma_*}{F_*} = \frac{\Gamma}{F} \frac{\sin\ell\Delta y/\ell\Delta y}{\cos\frac{\ell\Delta y}{2}} \tag{38}$$

and $(\sin\ell\Delta y/\ell\Delta y) \div \cos \ell\Delta y/2 \simeq 1$ in the range $0 \leq \ell\Delta y \leq \pi/2$. This means that we may follow a line along Γ_*/F_* = const. (dashed line) towards the origin to see how $\Omega c/\Omega a$ changes as Δy is reduced. Unfortunately, $\Delta y/\lambda$ also changes proportionately and so we must flip between 4b, 4c, and 4d while we are following a Γ_*/F_* = const. line towards the origin. With some manual dexterity, the result is seen (as expected): a reduction of Δy uniformly leads to greater accuracy of phase speeds. Figure 6 shows the same thing to be true for the explicit model. Also, Figures 8 and 9 show that the group velocities are also improved by reducing Δy.

A second objective of reduction of grid length is to be able to include smaller features in the calculation. Hopefully, the phase speed of the smallest well-resolved scale would remain of comparable accuracy as the grid length is reduced. For the semi-implicit model, this must be a limited objective since the smallest atmospheric scales represent gravity waves and they are a priori to be poorly calculated by the semi-implicit formulation. One must determine from physical principles at what point in the reduction of Δy this second objective is no longer valid. For now, let's consider it to be valid.

The semi-implicit stability criterion (28) implies that Δt need not be reduced as Δy is reduced. Let's consider how $\Omega c/\Omega a$ and $d\sigma_c/d\ell \div d\sigma_a/d\ell$ change as Δy is reduced with $\ell\Delta y$ and Δt held constant (i.e., Γ_* increases with F_* fixed). Figure 10 has been prepared to show a particular example. In this example, $F_* = 0.5$, $\Gamma_* = 1/32$ is the starting point. Also included are the changes to Ω_E/Ω_a and $d\sigma_E/d\ell \div d\sigma_a/d\ell$ under the same variation of Δy with $\ell\Delta y$ and Δt fixed. As expected, the explicit model becomes unstable when $\Gamma_*^2 + F_*^2 = 1$. The accuracy of the semi-implicit model does not change much until the waves considered fall near the gravity wave region. Then the accuracy falls sharply.

Actually it is not possible to leave the time step fixed while Δy is reduced in the semi-implicit model. This is because the basic wind speed has been neglected in the linear analysis. The stability criteria for the semi-implicit and explicit models should be replaced by something like the following:

$$0 \le \left(f^2 + \frac{u^2}{\Delta y^2}\right)\Delta t_c^{\,2} \le 1 \quad \text{semi-implicit} \tag{39}$$

and

$$0 \le \left(f^2 + \frac{c_*^2 + u^2}{\Delta y^2}\right)\Delta t_E^{\,2} \le 1 \text{ explicit} \tag{40}$$

where Δt_c and Δt_E are the time steps in the semi-implicit and explicit models.

It is rather difficult to see in general how the accuracy of the phase speeds and group velocities change as Δy is reduced while $(f^2 + u^2/\Delta y^2)\ t_c^2$ and $(f^2 + (u^2 + c_*^2)/\Delta y^2)\Delta t_E^2$ remain fixed, but a calculation from the same starting point as for Figure 10 ($F_* = 0.5$, $\Gamma_* = 1/32$) shows the accuracy to be greatly improved. It is presumed that this is true in general.

Another question is whether the time step advantage of the semi-implicit model is changed by a reduction of Δy. It is noted that

$$\frac{\Delta t_c}{\Delta t_E} = \left(\frac{f^2\Delta y^2 + C_*^2 + u^2}{f^2\Delta y^2 + u^2}\right)^{\frac{1}{2}} \frac{A_c}{A_E} \tag{41}$$

where $A_c = (f^2\Delta y^2 + u^2)\Delta t_c$ and $A_E = (f^2\Delta y^2 + u^2 + C_*^2)\Delta t_E$. Both A_c and and A_E are presumed to be held constant. They represent the proportion of the maximum allowable time step that is used. In the limit,

$\Delta y \to \infty$, it is seen that the stability limits for the two models become the same. Therefore, A_c and A_E must be close to each other. It will be assumed that they are identical. Thus,

$$\frac{\Delta t_c}{\Delta t_E} \simeq \left(\frac{f^2\Delta y^2 + C_*^2 + u^2}{f^2\Delta y^2 + u^2}\right) \tag{42}$$

Table 2 shows $\Delta t_c/\Delta t_E$ for some values of interest. It is the largest C_* and u that must be used in (42).

Table 2. $\Delta t_c/\Delta t_E$

$f = 1.0 \times 10^{-4}\ s^{-1}$, $C_* = 300$ m/s, $A_c = A_E$.

	$u = 50\ m\ s^{-1}$	$u = 100\ m\ s^{-1}$
$\Delta y \to \infty$	1.00	1.00
$\Delta y = 381$ km	4.88	2.98
$\Delta y = 190.5$ km	5.70	3.11
$\Delta y \to 0$	6.08	3.16

The effect of the maximum windspeed, u, is clearly illustrated by this example. It also shows that the time step advantage of the semi-implicit model increases slightly as Δy is reduced below "1 Bedient." However, once Δy is reduced to the point at which all desired scales are adequately resolved, it is most efficient to obtain additional accuracy by going to a higher order space differencing scheme rather than by further reduction of Δy.

b. Geostrophic adjustment

The gravity-inertia waves of the atmosphere act in a way to mutually adjust the mass and wind fields to an approximate geostrophic balance. In a numerical model of the atmosphere, much of the imbalance can be described as noise, since it is unrelated to any physical generator of imbalances. It is usually desirable to eliminate the noise by smoothing or diffusion. At the same time, we might want to try to retain any physical adjustment process. Table 3 lists some physical phenomena that are believed to produce appreciable imbalances in the atmosphere. The table lists the phenomena, their typical wavelength, C_*, and $\Gamma/F = \ell c^*/f$.

Table 3.

Phenomenon	λ(m)	C_*(m/s)	Γ/F
Rapidly deepening systems	2×10^6	300, 60	9, 1.8
Low-level jet	5×10^5	10	1.2
Jet stream	10^6	10	.6
Mountain waves	2×10^4	30	90
Thunderstorms	2×10^4	50	150
Boundary layer phenomena	5×10^5	10	1.2
Winds with large curvature	2×10^6	60	1.8

Those phenomena in the table with $\Gamma/F \leq 1$ will be treated nearly the same by an explicit or semi-implicit model, provided $\Delta y/\lambda << 1$. It is the phenomena with $\Gamma/F > 1$ that are of concern here. Within this class are rapidly deepening systems, low-level jet, mountain waves, thunderstorms, boundary layer phenomena, and winds with large curvature (supergeostrophic winds). Our maximum time step will be determined by which of these phenomena we may wish to calculate accurately. At present there is no agreement on whether the gravity waves set up by imbalances need to be accurately calculated. Some experiments with the semi-implicit model are designed to make this decision. Attention is again drawn to the fact that short grid length waves have group velocities that are small or negative. This feature is not inevitable with all models, however. (See Mesinger and Arakawa, 1977, p. 43 ff.)

5. Solutions for C_*

Table 4 shows the values of $|C_*|$ for a six-layer model with Standard Atmosphere temperatures. The model top is at 100 mb and the layers have equal pressure thicknesses. Figure 11 shows the shape of the eigenvectors. Their shapes are very similar to those of empirical orthogonal functions derived from geopotentials. However, the first empirical function peaks more strongly near 200 mb. The model structure shown here will be used in the semi-implicit experiments of geostrophic adjustment.

Table 4. $|C_*|$ for 6-layer model

Mode	$\|C_*\|$ (m/s)
1	290.78
2	62.69
3	26.33
4	14.54
5	8.16
6	3.76

One largely unanswered question in numerical modeling is the amount of vertical resolution needed. This linear analysis can be used to shed some light on this problem. It was felt that reasonably few layers would be sufficient to give good phase speeds for the first few modes for a Standard Atmosphere temperature profile, making this profile a rather uninteresting one for experimentation. Therefore, an actual atmospheric sounding was used for this question instead. The data is for Greensboro, N.C., 12Z 9 Dec. 1973. Figure 12 shows the temperature profile. It includes stable layers near 700 mb and 400 mb, which would be missed in models with gross vertical resolution. Figure 13 shows how the values of $|C_*|$ vary with the number of model layers (6, 10, 20) for the first several modes. It is found that the values of $|C_*|$ do not vary by more than 10% for the first four modes for ten or more layers.

Figure 14 shows how the first six eigenvectors change as the number of layers is increased from 6 to 10 to 20. Figure 15 shows the errors in the temperature profiles for 6, 10, and 20 layer models. The temperature is assumed to vary linearly with $\ln p$ to obtain differences with the observed temperatures. Already a 6-layer model presents the gross characteristics of the temperature profile, including a suggestion of the stable layer near 700 mb. Naturally, the 10 and 20 layer models do much better. However, even the 20-layer model has only a suggestion of the stable layer near 400 mb. The conclusions to be drawn are left to the reader. Clearly, the conclusions will depend upon the phenomenon to be modeled.

6. Summary

This note has shown the linearized perturbation equations for a two-dimensional semi-implicit forecast model on an f-plane. From these equations the frequency equation was derived. The vertical structure and eigenvalues of the vertical matrix (which are phase speeds squared) were shown for a Standard Atmosphere temperature profile. The group velocities were also shown. For comparison, the same parameters were calculated for an explicit model with centered time differencing.

The results were applied to a discussion of grid length reduction, geostrophic adjustment, and vertical resolution. It was emphasized that the conclusions to be drawn depend critically upon the intended model use. Some conclusions will be drawn in the future from nonlinear numerical experiments with the semi-implicit model in comparison with the explicit model.

Acknowledgments

I would like to thank Joe Gerrity and Cliff Dey for valuable discussions. While not explicitly cited in the text, all materials in the reference list were used for background material. I am indebted to Hans Økland for general discussion on geostrophic adjustment.

References

Blumen, W., 1972, Geostrophic Adjustment, Reviews of Geophysics and Space Physics, 10, No. 2, pp. 485-528.

Cahn, A., 1945, An investigation of the free oscillations of a simple current system, J. Met., 2, No. 2, pp. 113-119.

Mesinger, F., and A. Arakawa, 1976, Numerical Methods Used in Atmospheric Models, Vol. 1, GARP Publications Series, No. 17, 64 pp.

Økland, H., 1970, On the adjustment toward balance in primitive equation weather prediction models, MWR, Vol. 98, No. 4, p. 271-279.

Økland, H., 1972, On the balance, initialization and data assimilation in primitive equation prediction models, JAS, 29, p. 641-648.

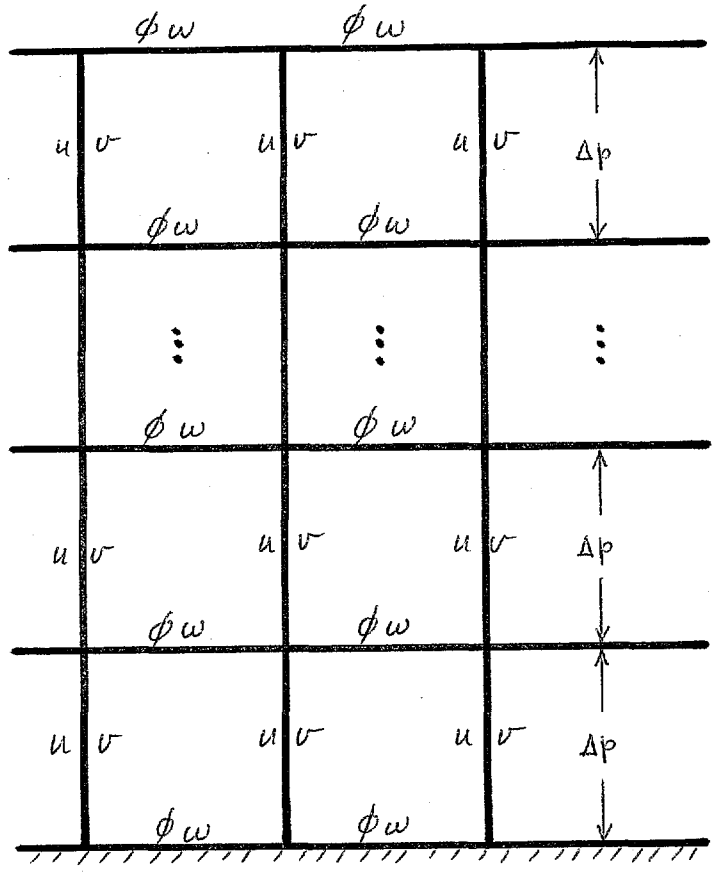
$\phi\omega$
$\phi\omega$
u v
u v
u v
Δp
$\phi\omega$
$\phi\omega$
$\phi\omega$
$\phi\omega$
u v
u v
u v
Δp
$\phi\omega$
$\phi\omega$
u v
u v
u v
Δp
$\phi\omega$
$\phi\omega$

Fig. 1

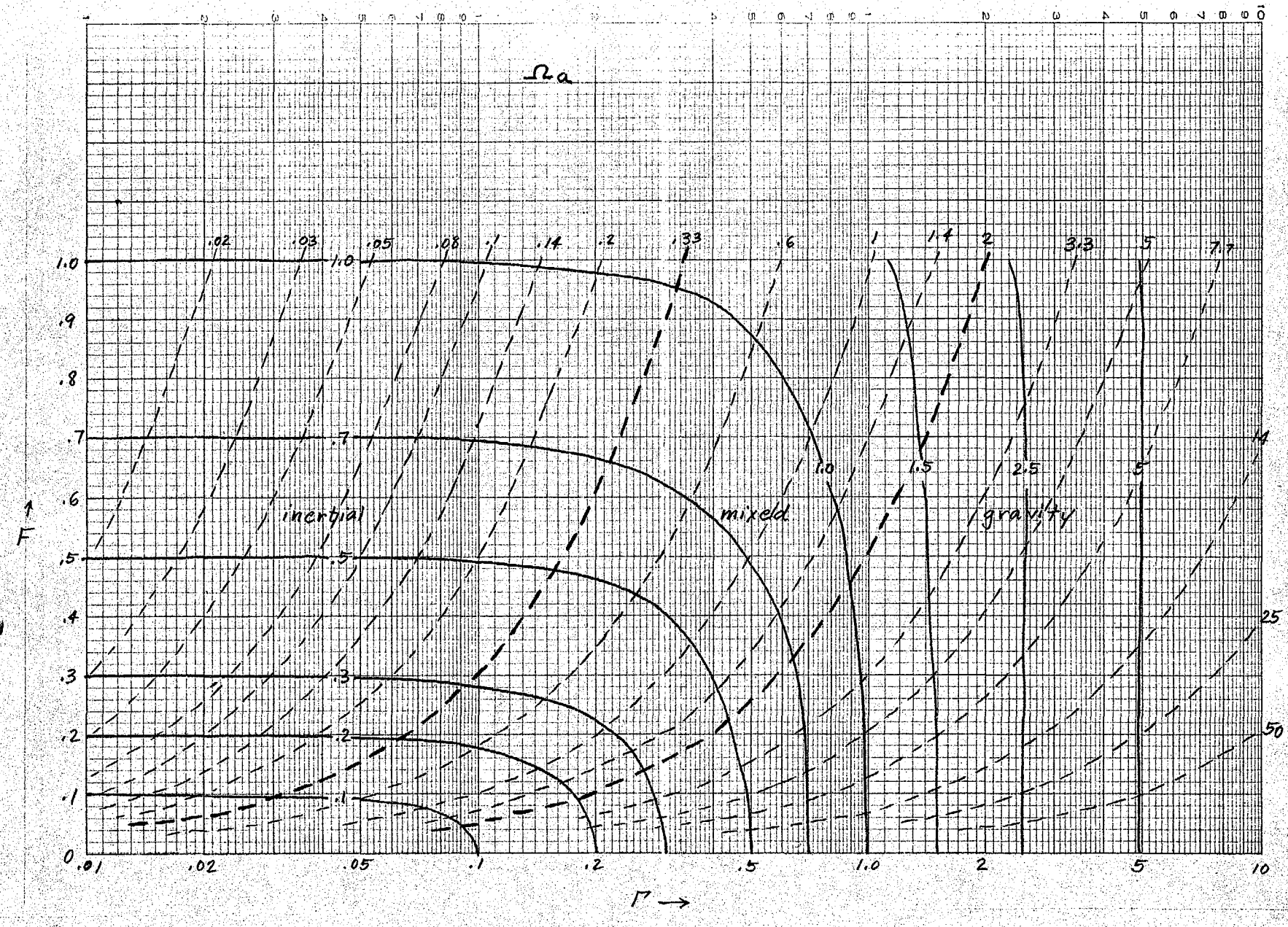
Ωa
F
Γ →
inertial
mixed
gravity
.02
.03
.05
.08
.1
.14
.2
.33
.6
1
1.4
2
3.3
5
7.7
1.0
.7
.5
.3
.2
.1
1.0
1.5
2.5
5
14
25
50
0
.01
.02
.05
.1
.2
.5
1.0
2
5
10

Fig. 2

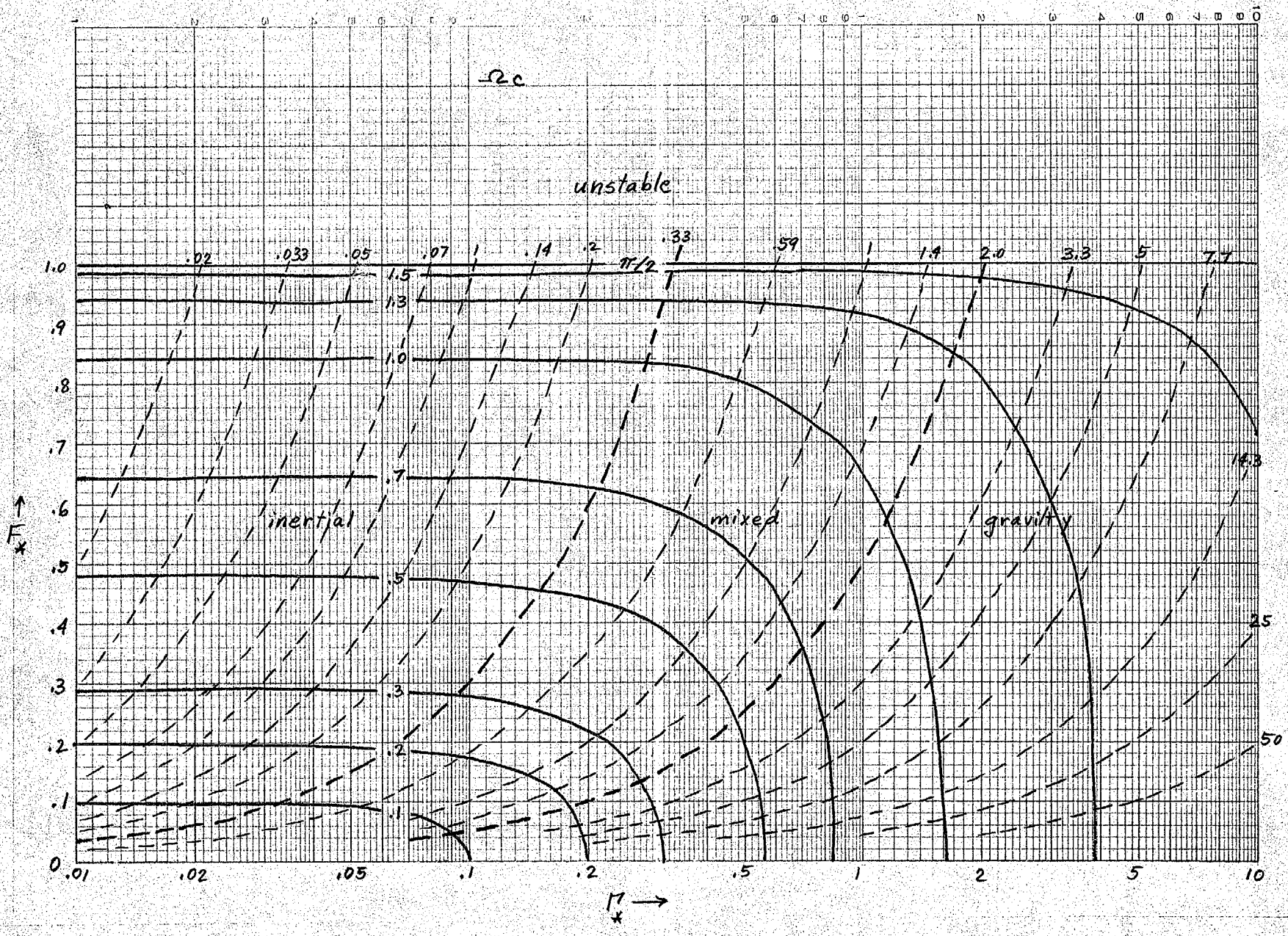

Fig. 3

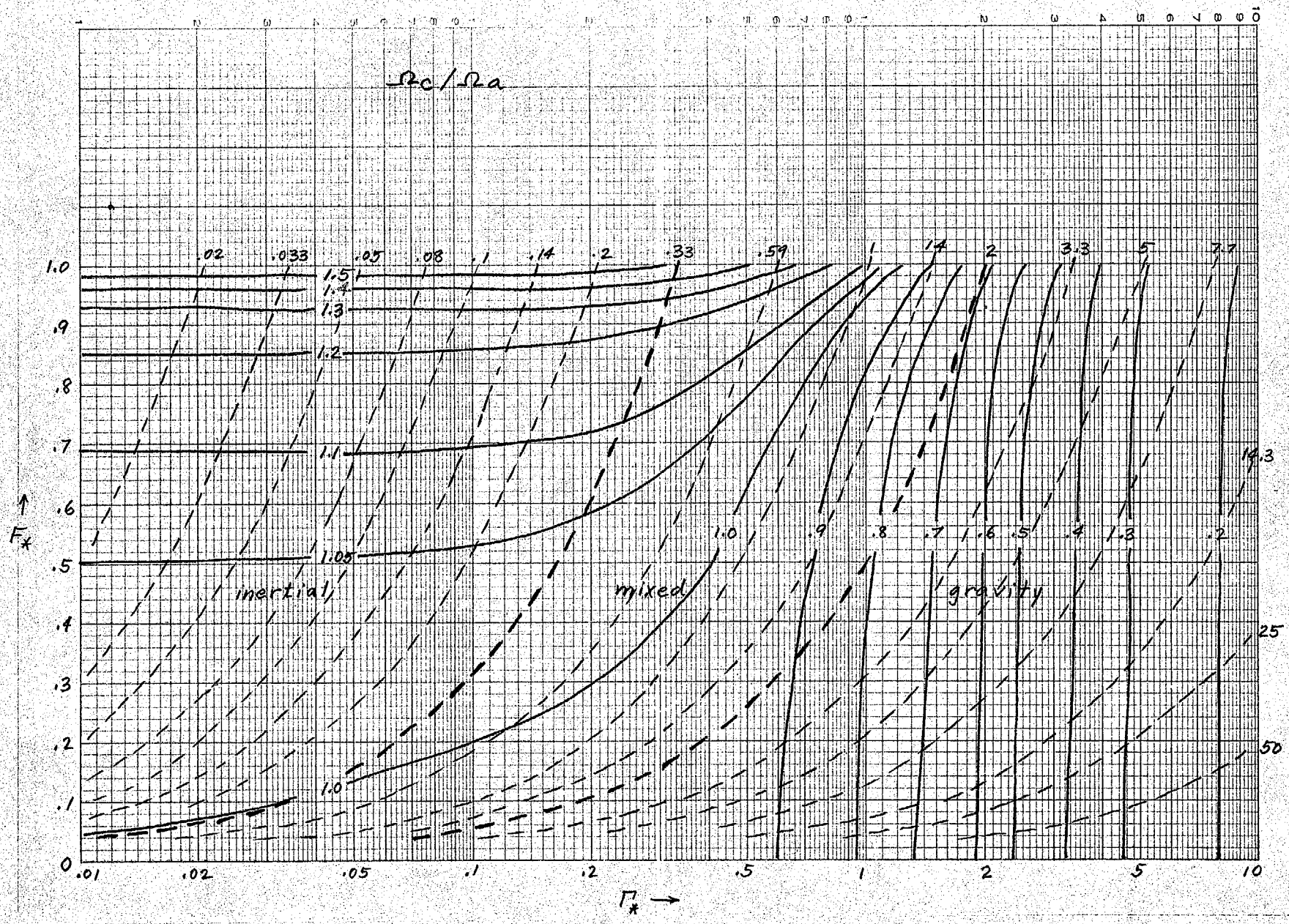
Ωc/Ωa
inertial
mixed
gravity
F*
Γ*
1.0
.9
.8
.7
.6
.5
.4
.3
.2
.1
0
.01
.02
.05
.1
.2
.5
1
2
5
10
1.5
1.4
1.3
1.2
1.1
1.05
1.0
.02
.033
.05
.08
.1
.14
.2
.33
.59
1
1.4
2
3.3
5
7.7
14.3
25
50

Fig. 4a

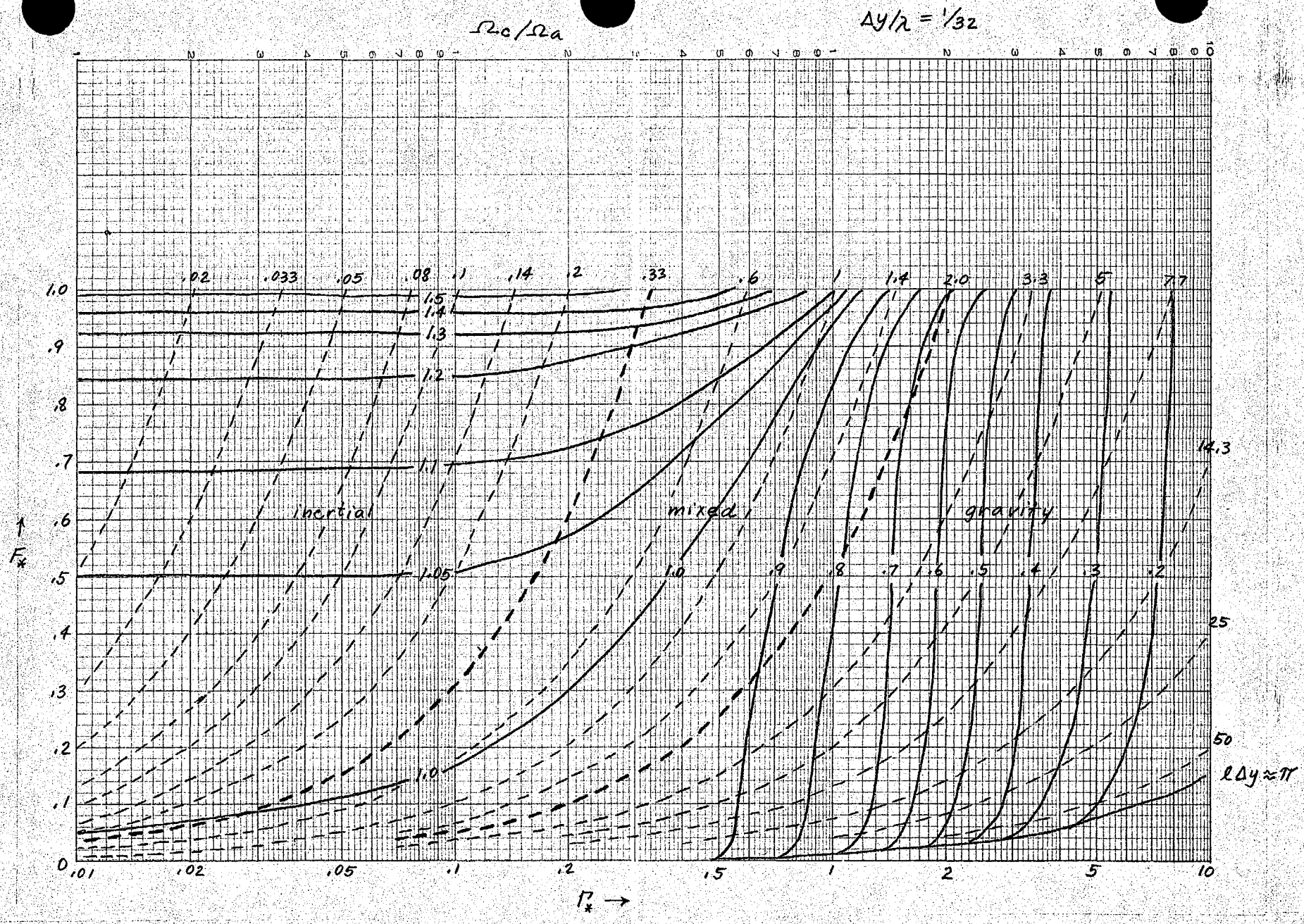
NO. 340R-L310 DIETZGEN GRAPH PAPER
SEMI-LOGARITHMIC 3 CYCLES X 70 DIVISI
EUGENE DIETZGEN CO.
MADE IN U.S.A.
Ωc/Ωa
Δy/λ = 1/32
.02
.033
.05
.08
.1
.14
.2
.33
.6
1
1.4
2.0
3.3
5
7.7
14.3
25
50
ℓΔy ≈ π
1.5
1.4
1.3
1.2
1.1
1.05
1.0
.9
.8
.7
.6
.5
.4
.3
.2
inertial
mixed
gravity
F*
Γ*
.01
.02
.05
.1
.2
.5
1
2
5
10

Fig. 4b

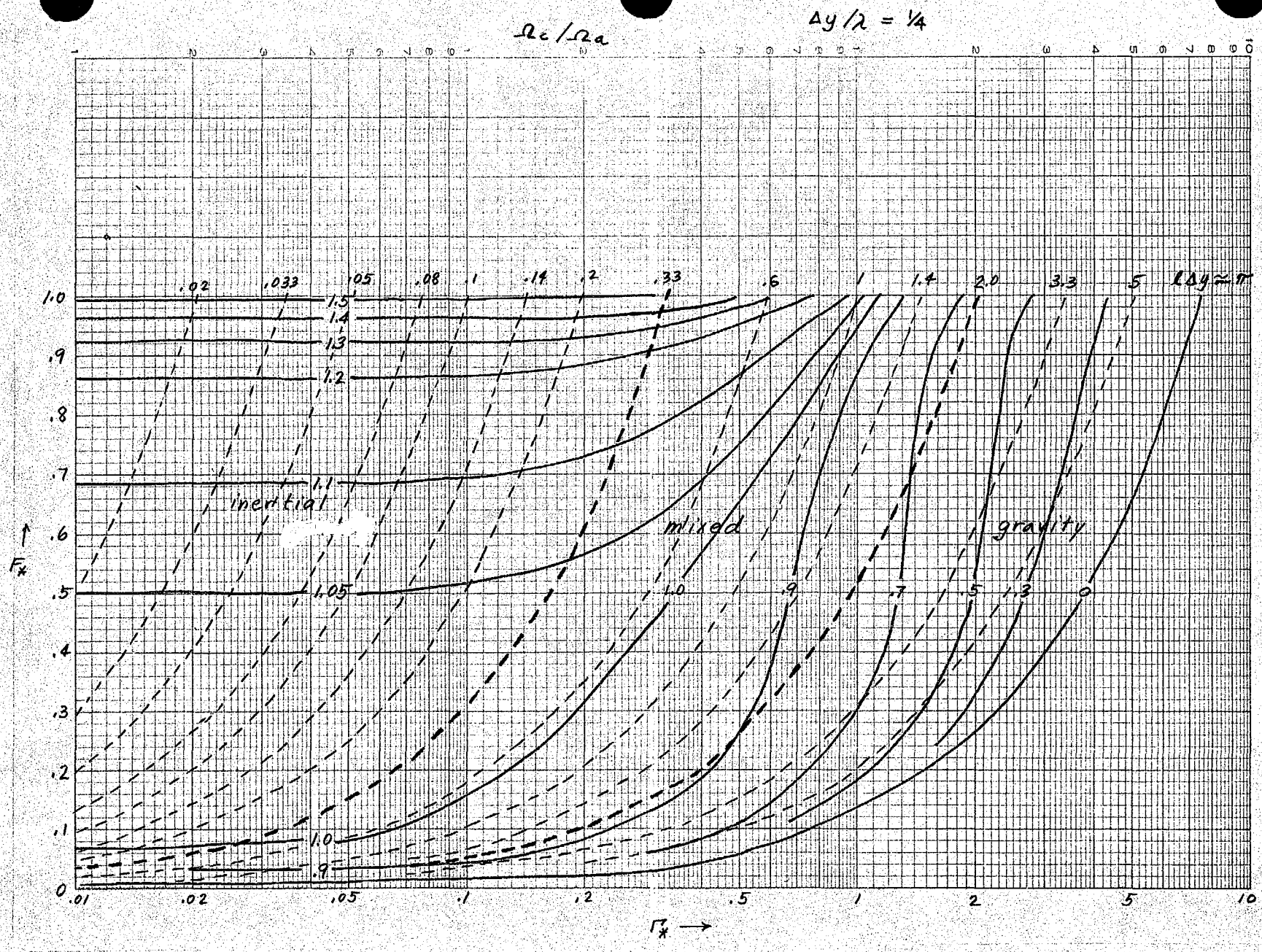

Fig. 4c

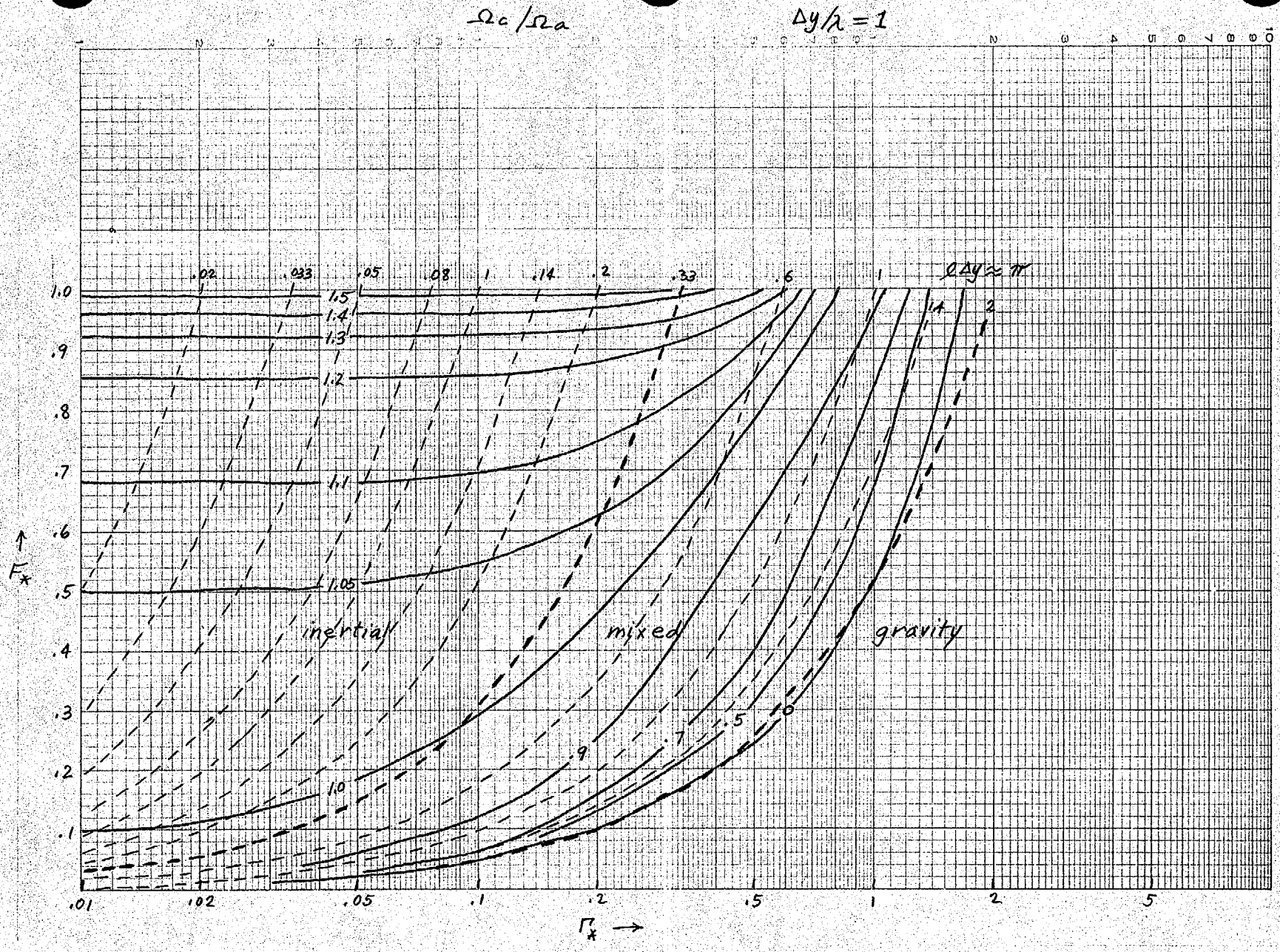
NO. 340R-L310 DIETZGEN GRAPH PAPER
SEMI-LOGARITHMIC 3 CYCLES X 70 DIVISIONS
EUGENE DIETZGEN CO.
MADE IN U.S.A.
Ωc/Ωa
Δy/λ = 1
Δy ≈ π
inertial
mixed
gravity
F*
Γ*

Fig. 4d

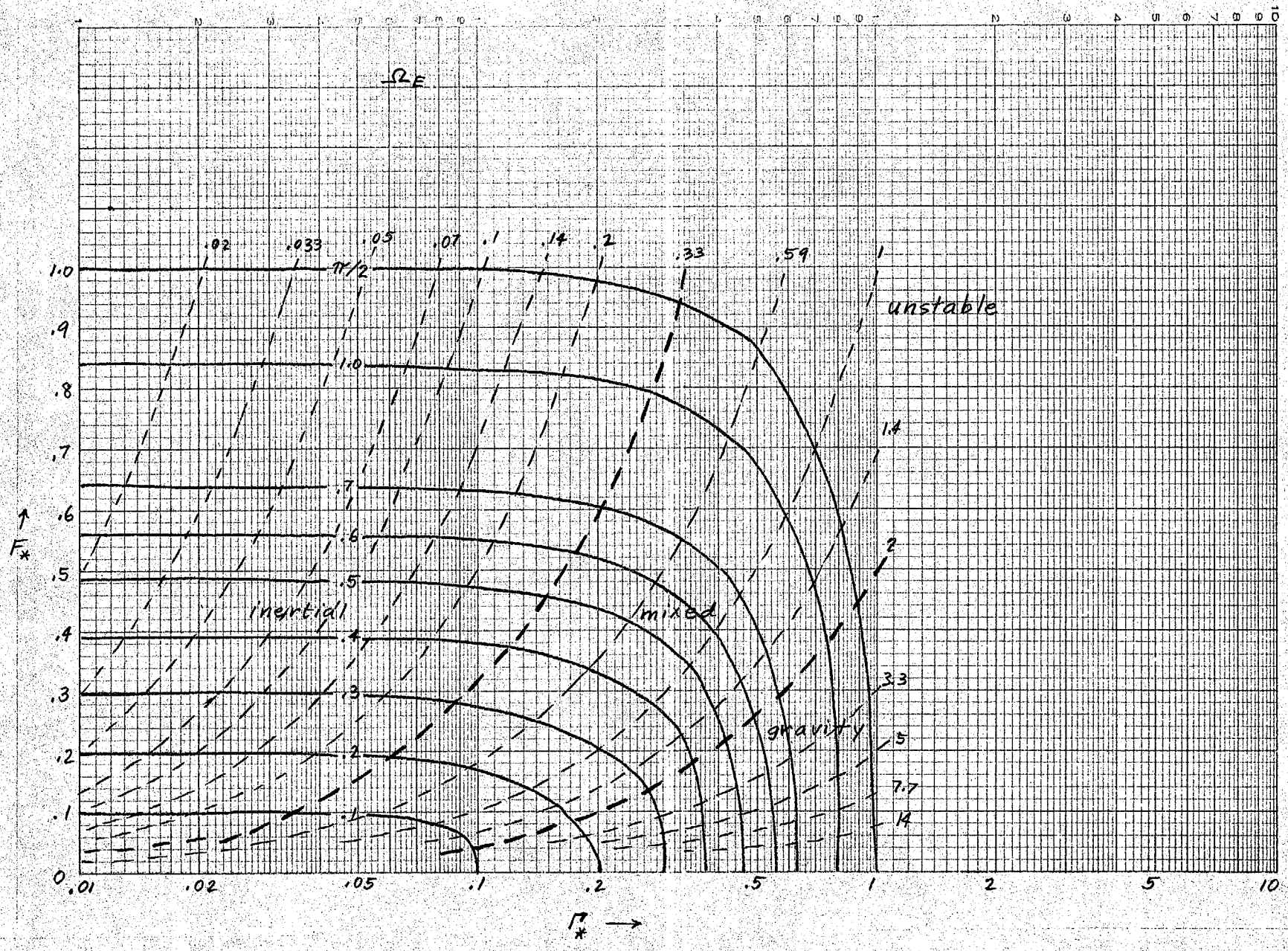

Fig. 5

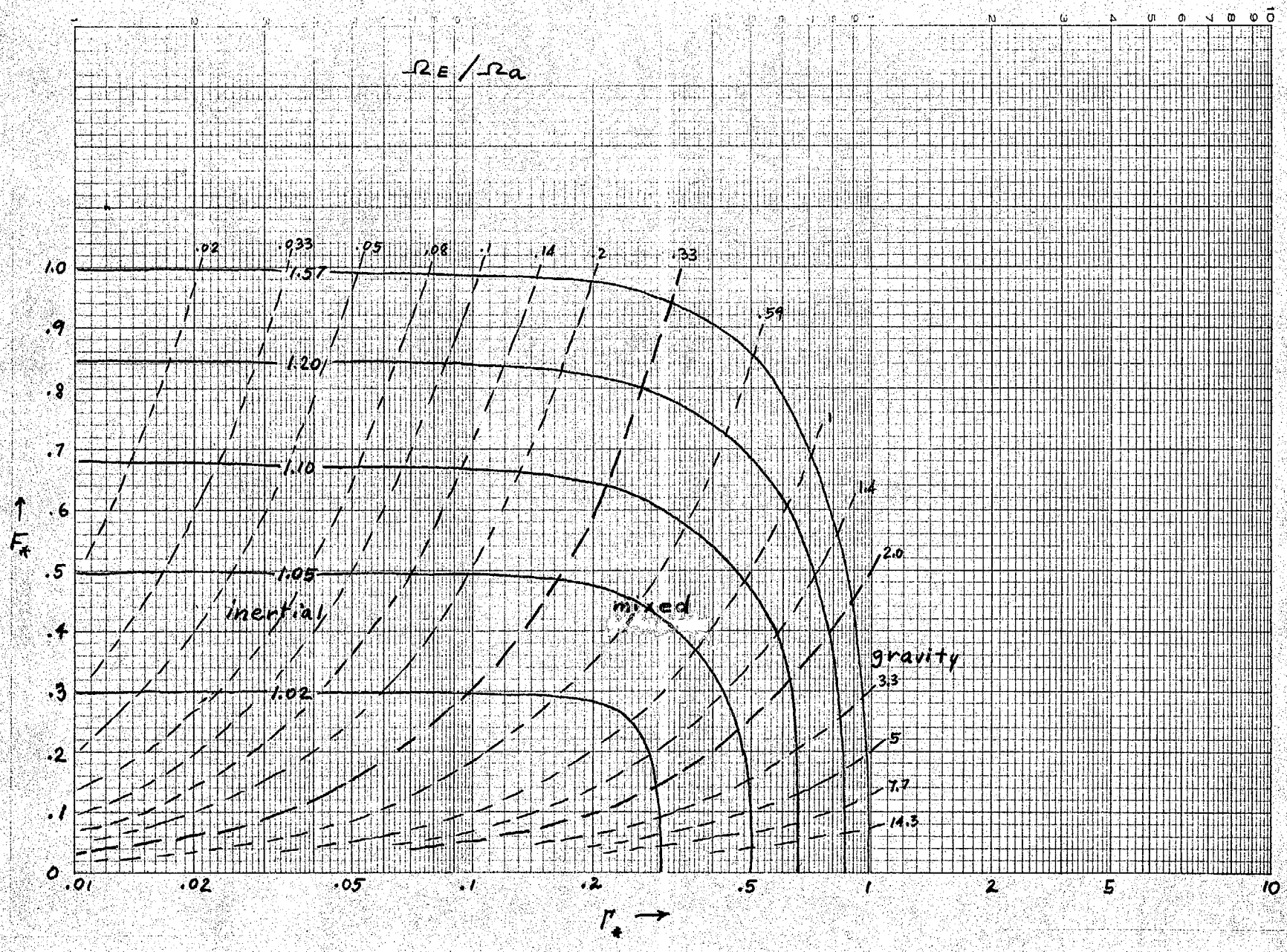

Fig. 6a

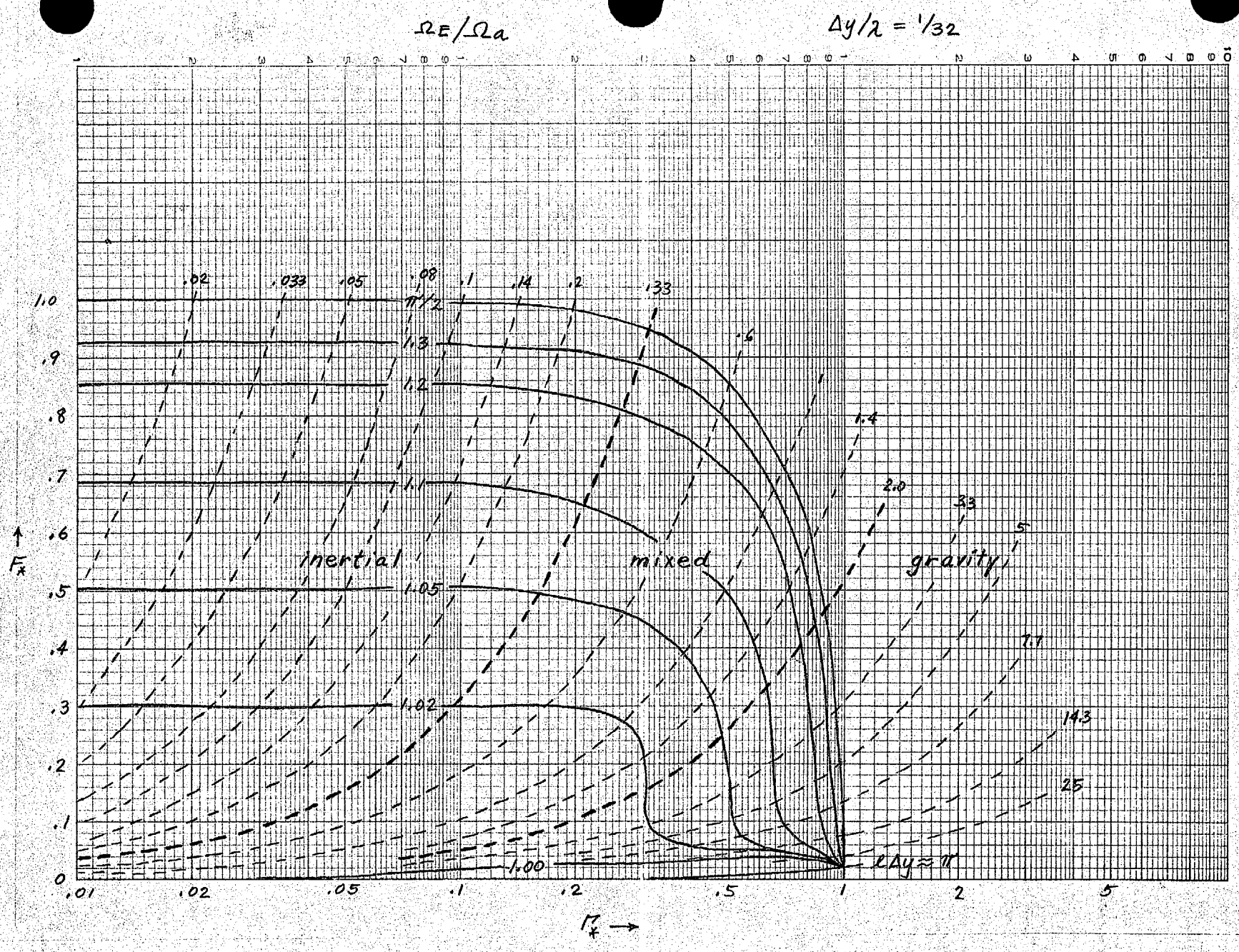
NO. 340R-L310 DIETZGEN GRAPH PAPER
SEMI-LOGARITHMIC 3 CYCLES X 70 DIVISIONS
EUGENE DIETZGEN CO.
MADE IN U.S.A.
Ω_E/Ω_a
$\Delta y/\lambda = 1/32$
F_*
Γ_*
inertial
mixed
gravity
$\ell\Delta y \approx \pi$
.02
.033
.05
.08
.1
.14
.2
.33
.6
1.4
2.0
3.3
5
7.1
14.3
25
$\pi/2$
1.3
1.2
1.1
1.05
1.02
1.00
1.0
.9
.8
.7
.6
.5
.4
.3
.2
.1
0
.01
.02
.05
.1
.2
.5
1
2
5

Fig. 6b

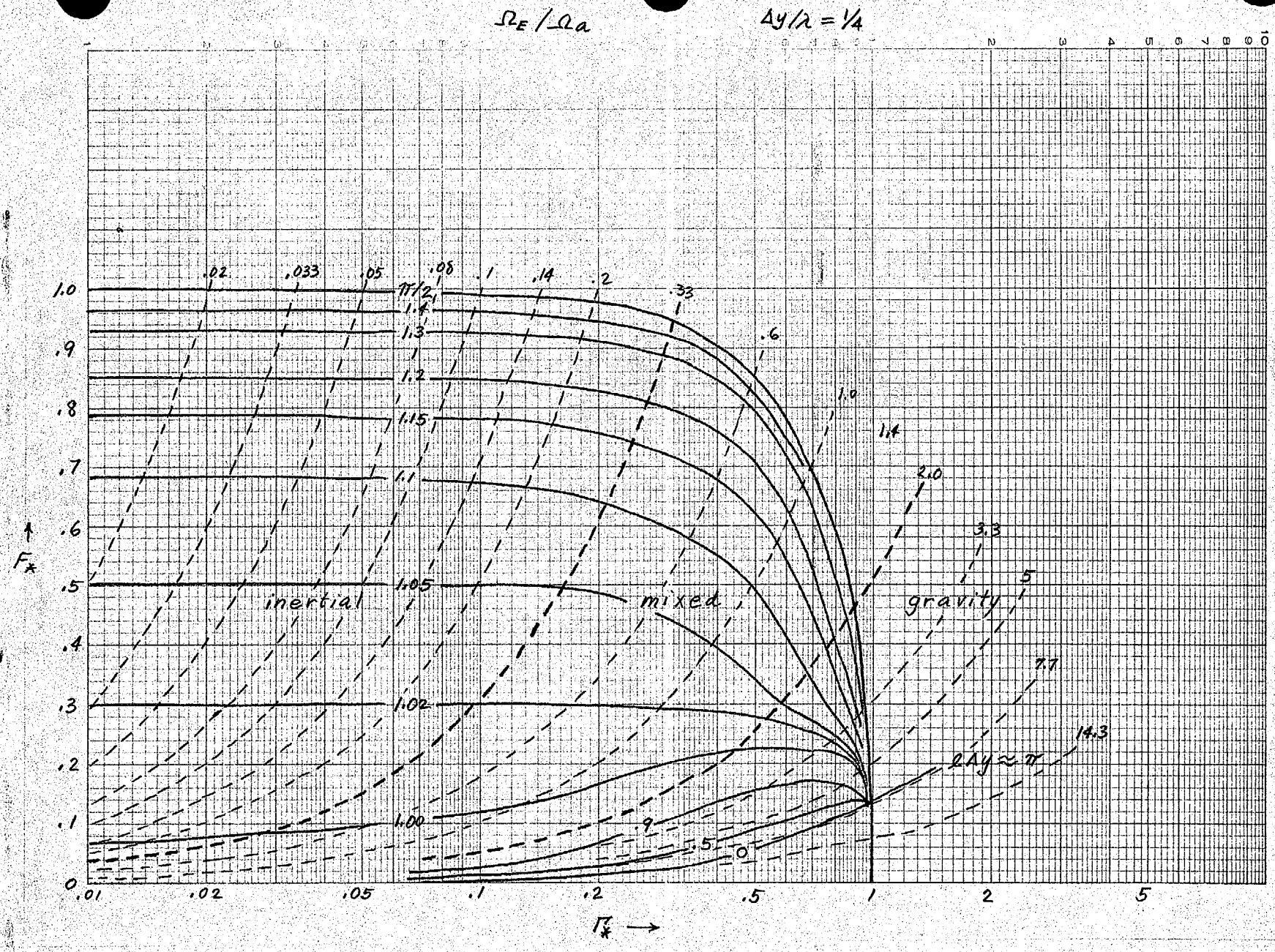

Fig. 6c

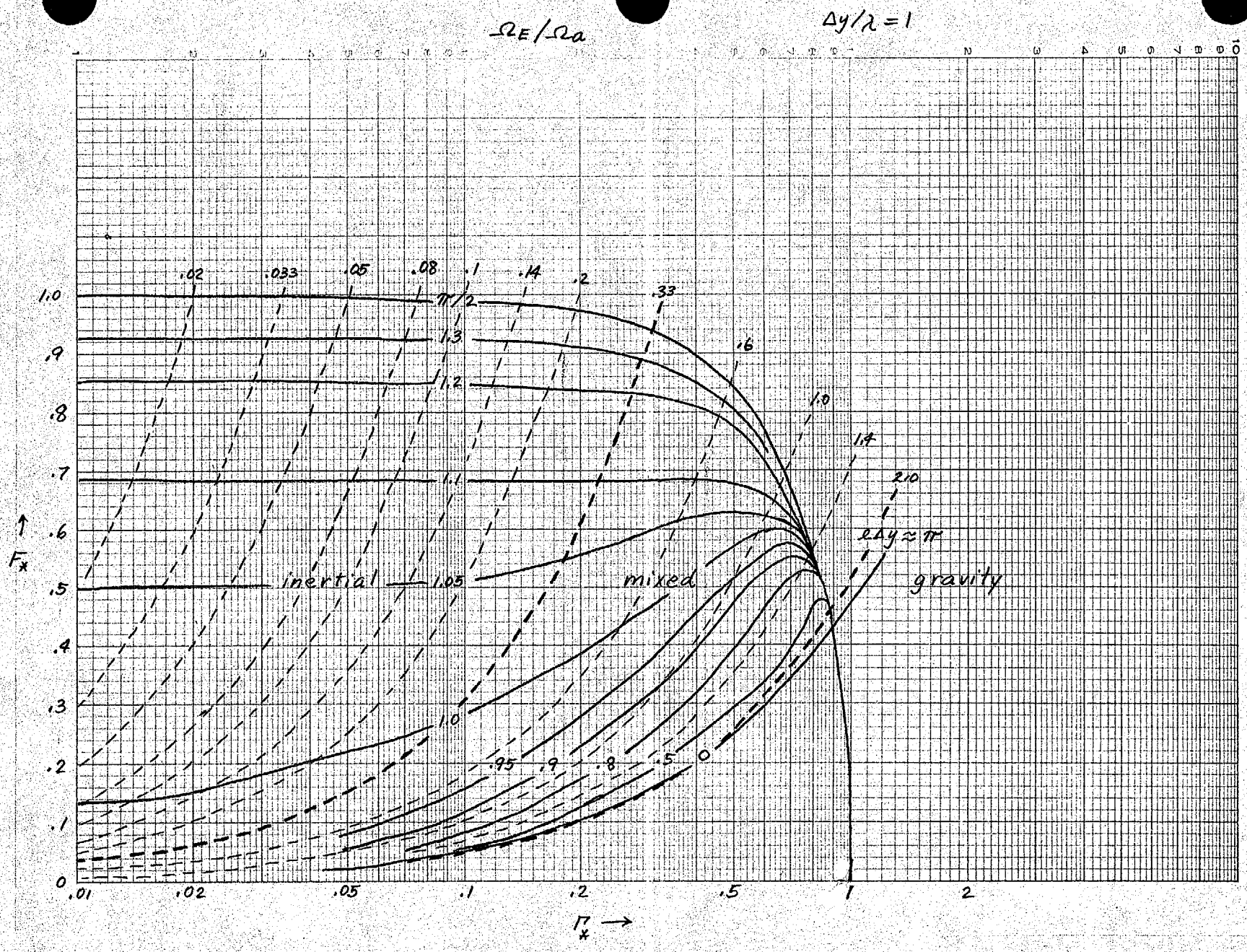
NO. 340R-L310 DIETZGEN GRAPH PAPER
SEMI-LOGARITHMIC 3 CYCLES X 70 DIVISIONS
EUGENE DIETZGEN CO.
MADE IN U.S.A.
Ω_E/Ω_a
$\Delta y/\lambda = 1$
F_x
Γ_x
inertial
mixed
gravity
$\ell\Delta y \approx \pi$
$\pi/2$
1.3
1.2
1.1
1.05
1.0
.95
.9
.8
.5
0
.02
.033
.05
.08
.1
.14
.2
.33
.6
1.0
1.4
2.0
.01
.02
.05
.1
.2
.5
1
2

Fig. 6d

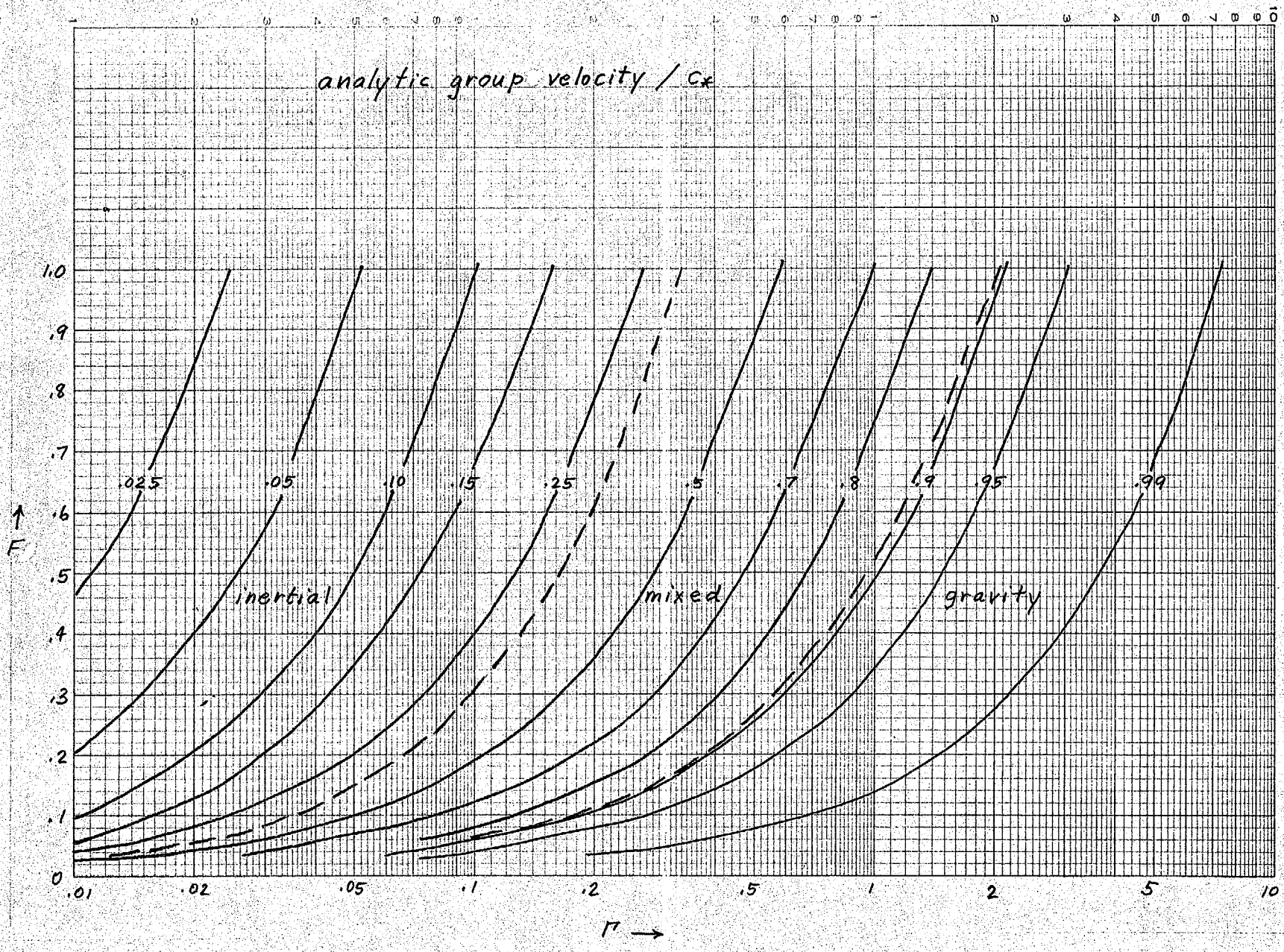
NO. 340R-L310 DIETZGEN GRAPH PAPER
SEMI-LOGARITHMIC 3 CYCLES X 70 DIVISIONS
EUGENE DIETZGEN CO.
MADE IN U.S.A.
analytic group velocity / c*
.025
.05
.10
.15
.25
.5
.7
.8
.9
.95
.99
inertial
mixed
gravity
F
Γ
1.0
.9
.8
.7
.6
.5
.4
.3
.2
.1
0
.01
.02
.05
.1
.2
.5
1
2
5
10

Fig. 7

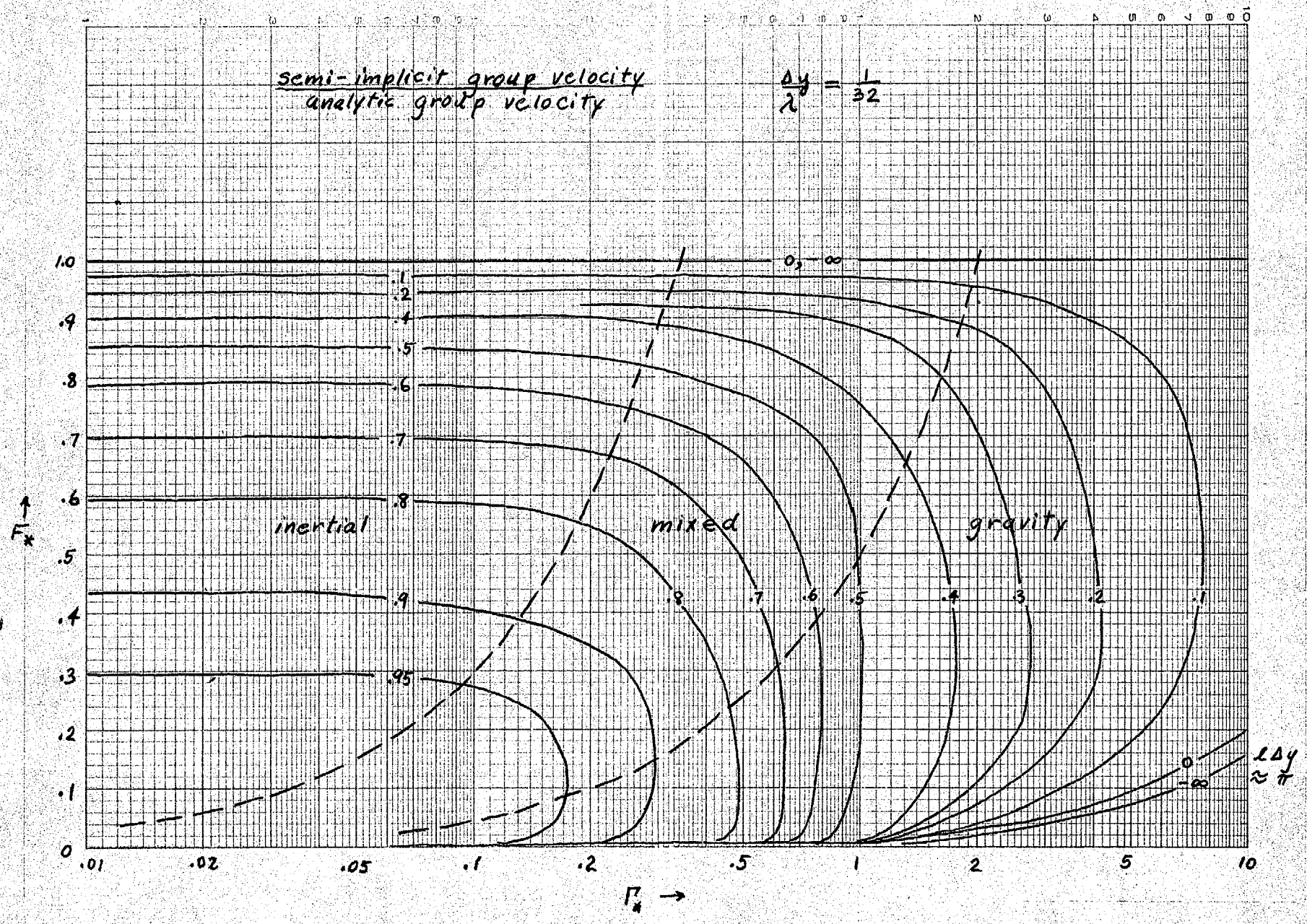

Fig. 8a

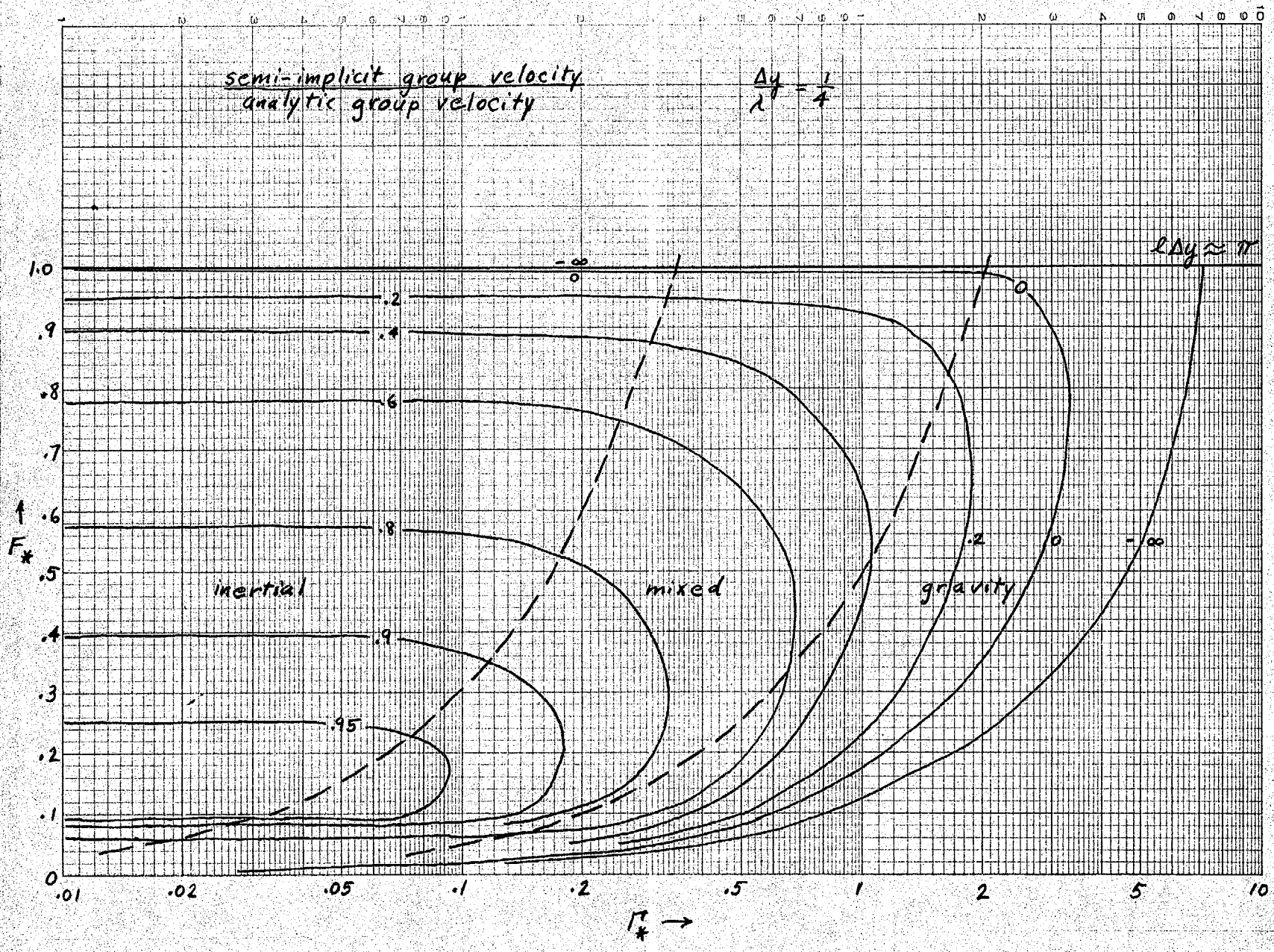

Fig. 8b

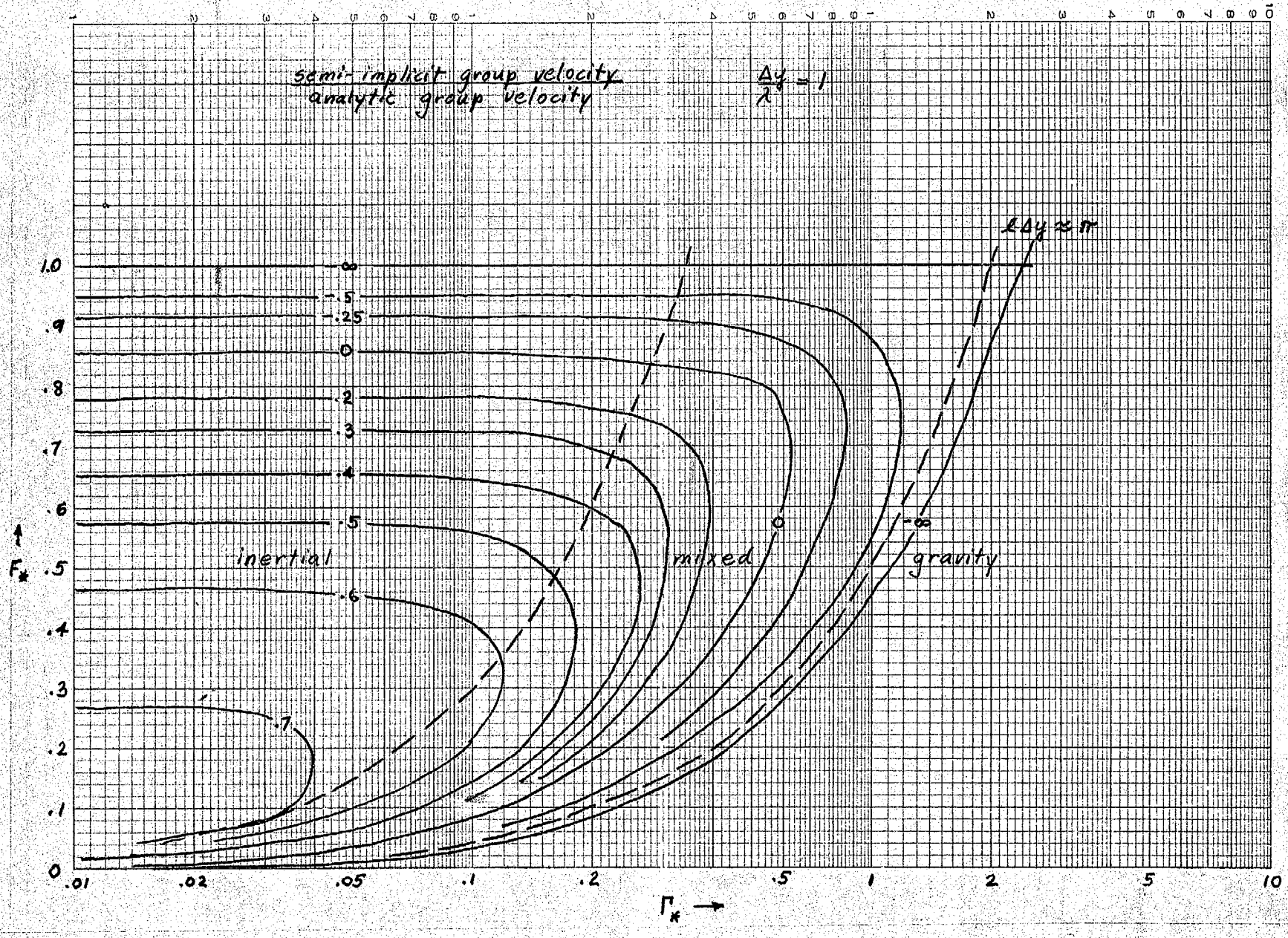

Fig. 8c

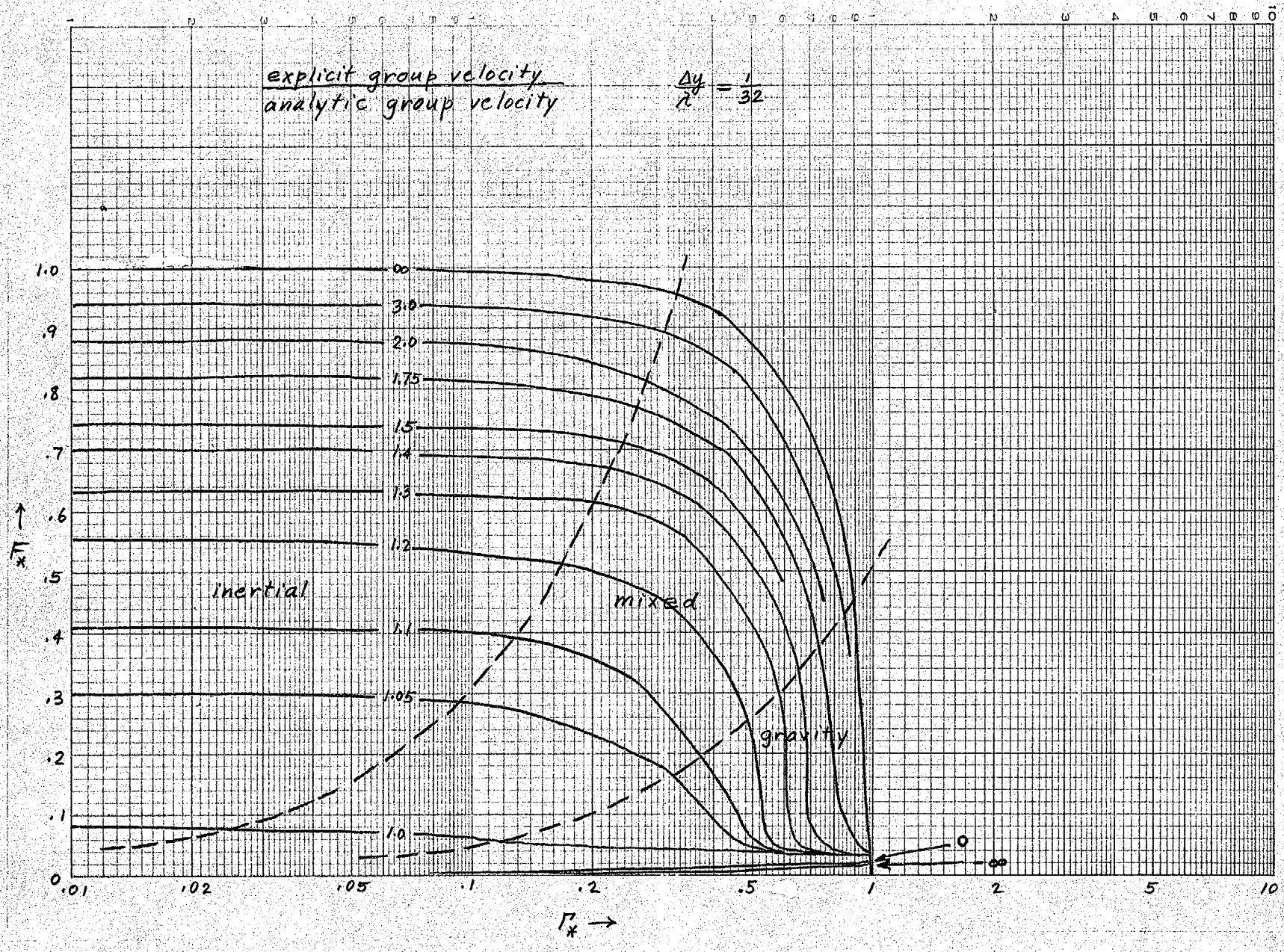

Fig. 9a

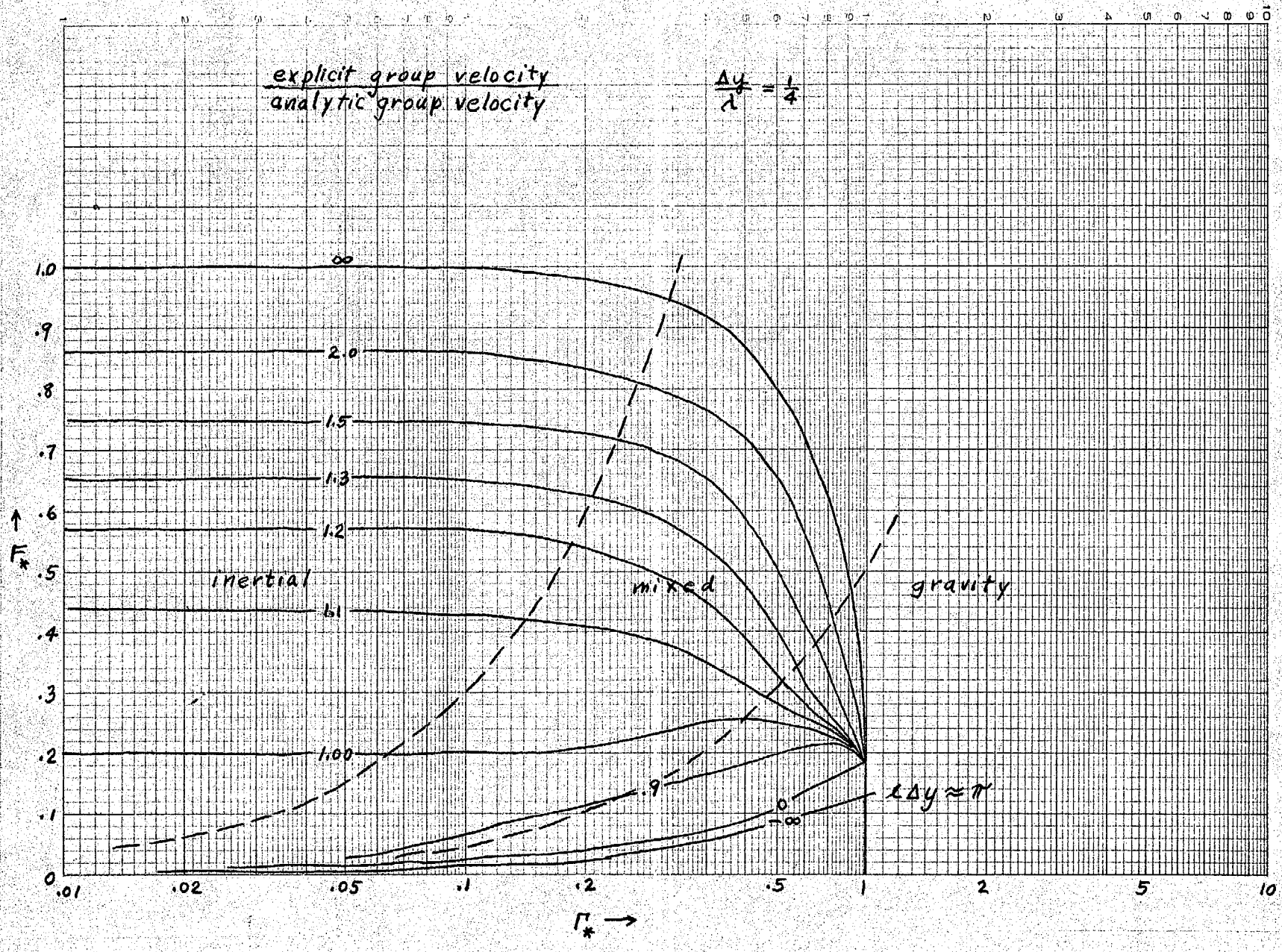

Fig. 9b

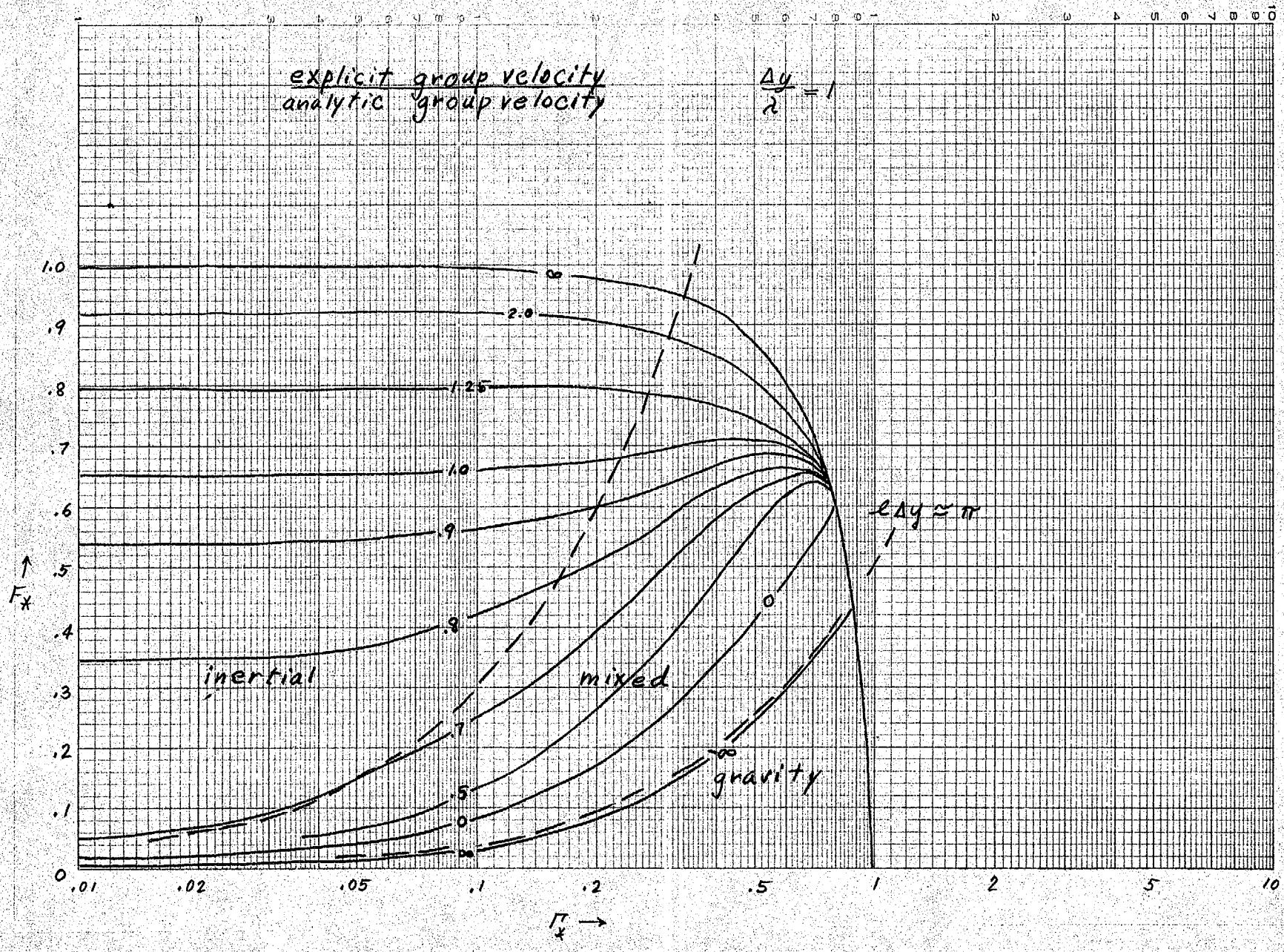

Fig. 9c

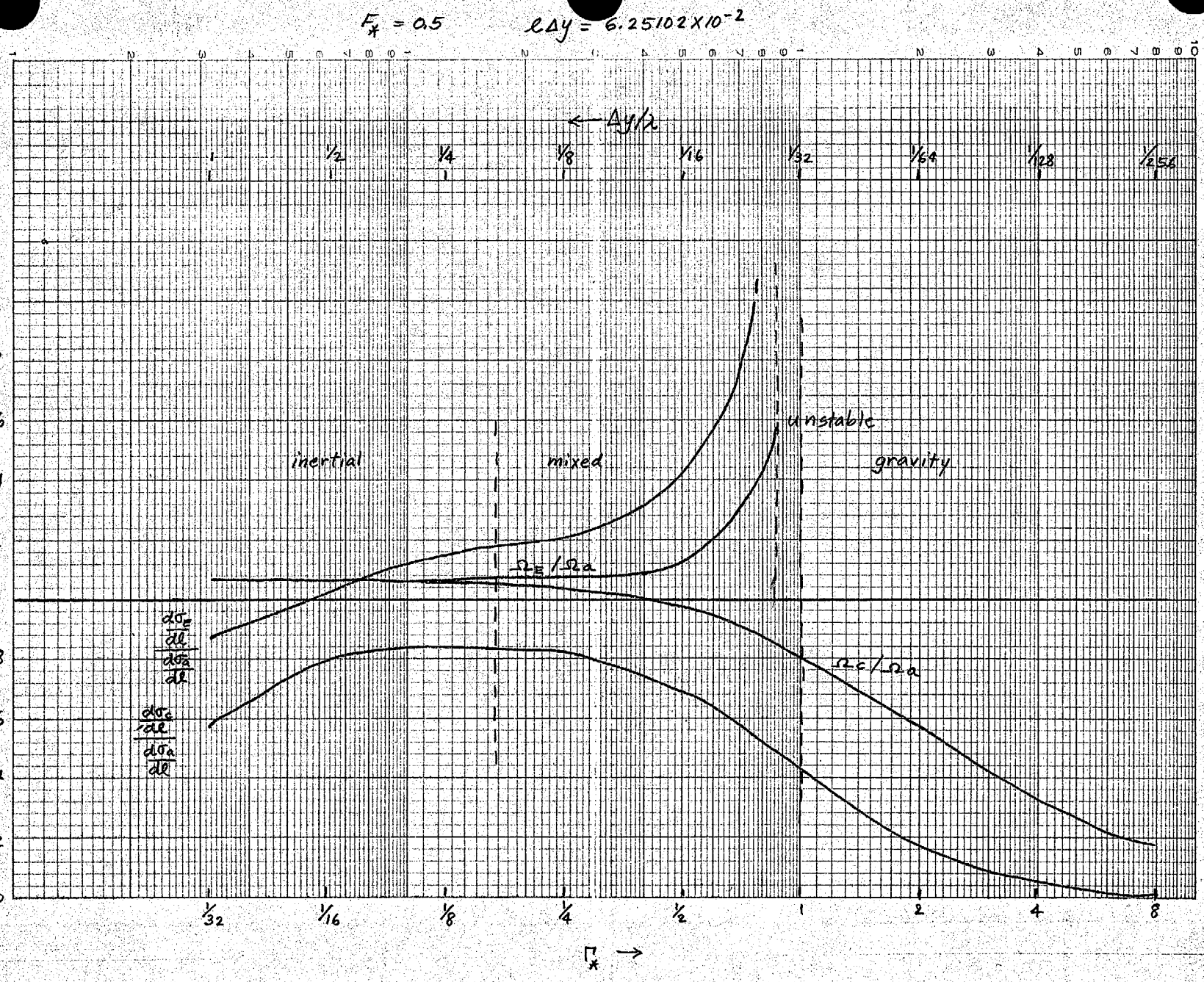

Fig. 10

Eigenvector Structure, Standard Atmosphere

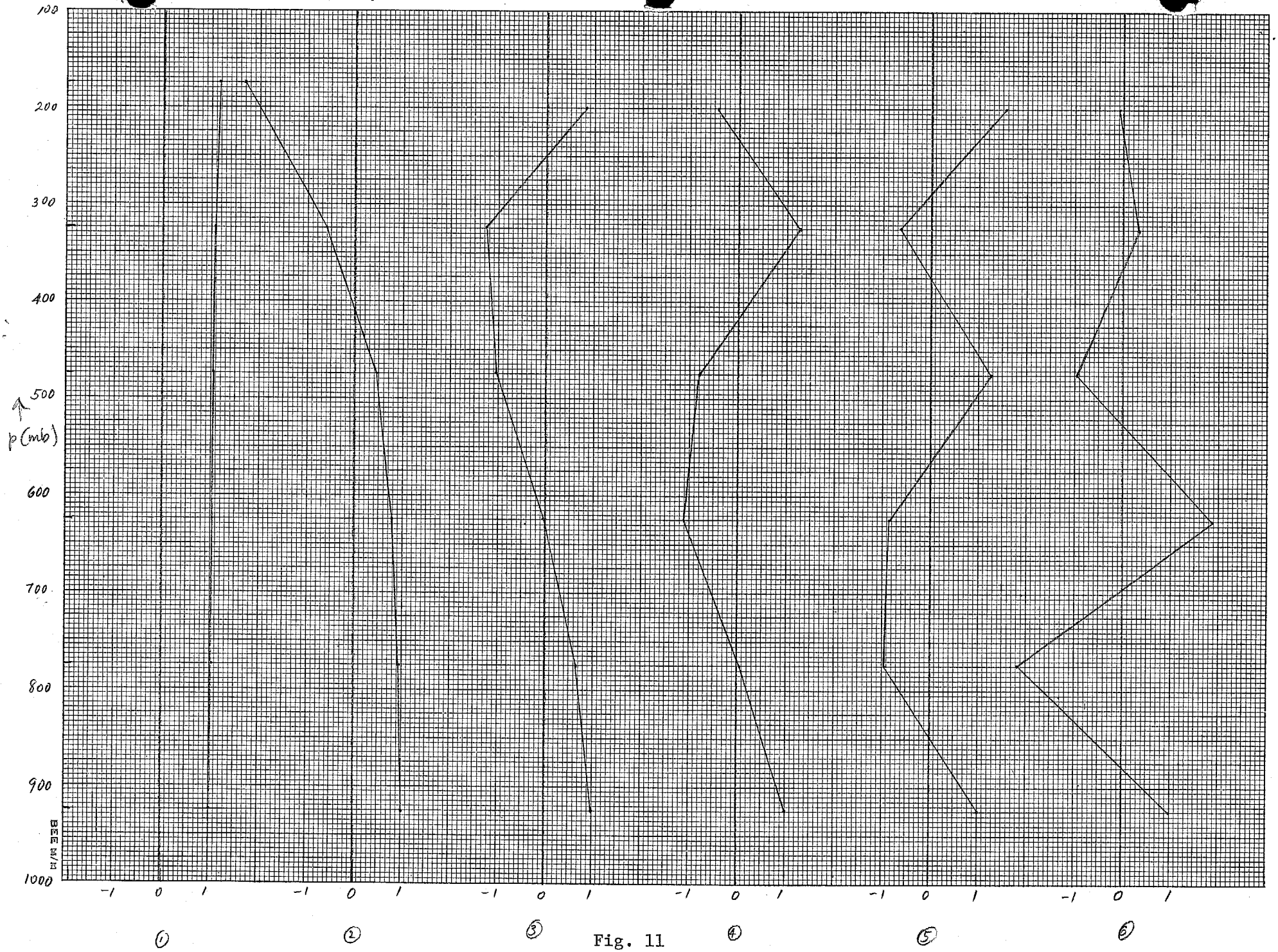

Fig. 11

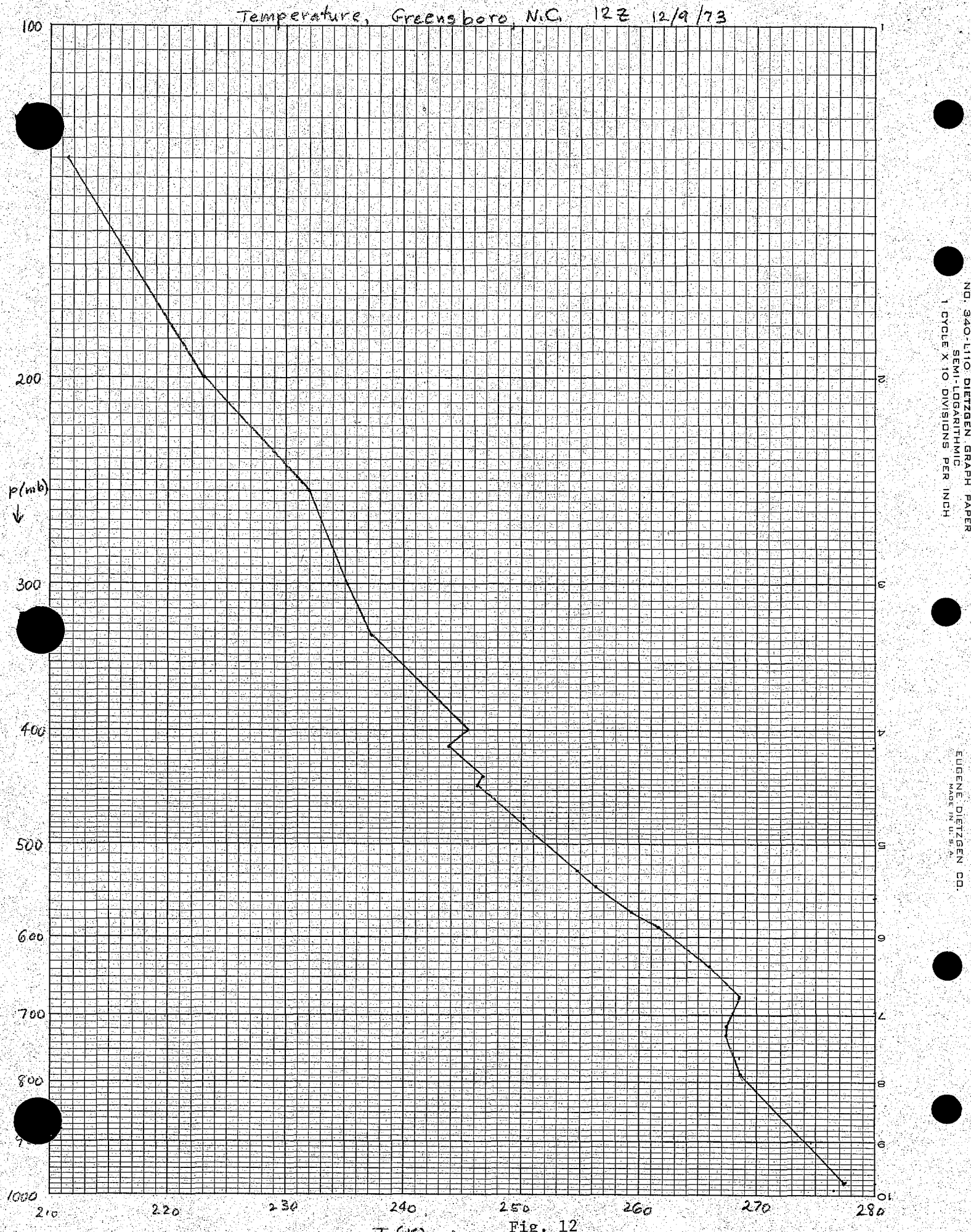
Temperature, Greensboro, N.C. 12Z 12/9/73
100
200
300
400
500
600
700
800
900
1000
p(mb)
210
220
230
240
250
260
270
280
T (K)
NO. 340-L110 DIETZGEN GRAPH PAPER
SEMI-LOGARITHMIC
1 CYCLE X 10 DIVISIONS PER INCH
EUGENE DIETZGEN CO.
MADE IN U.S.A.

Fig. 12

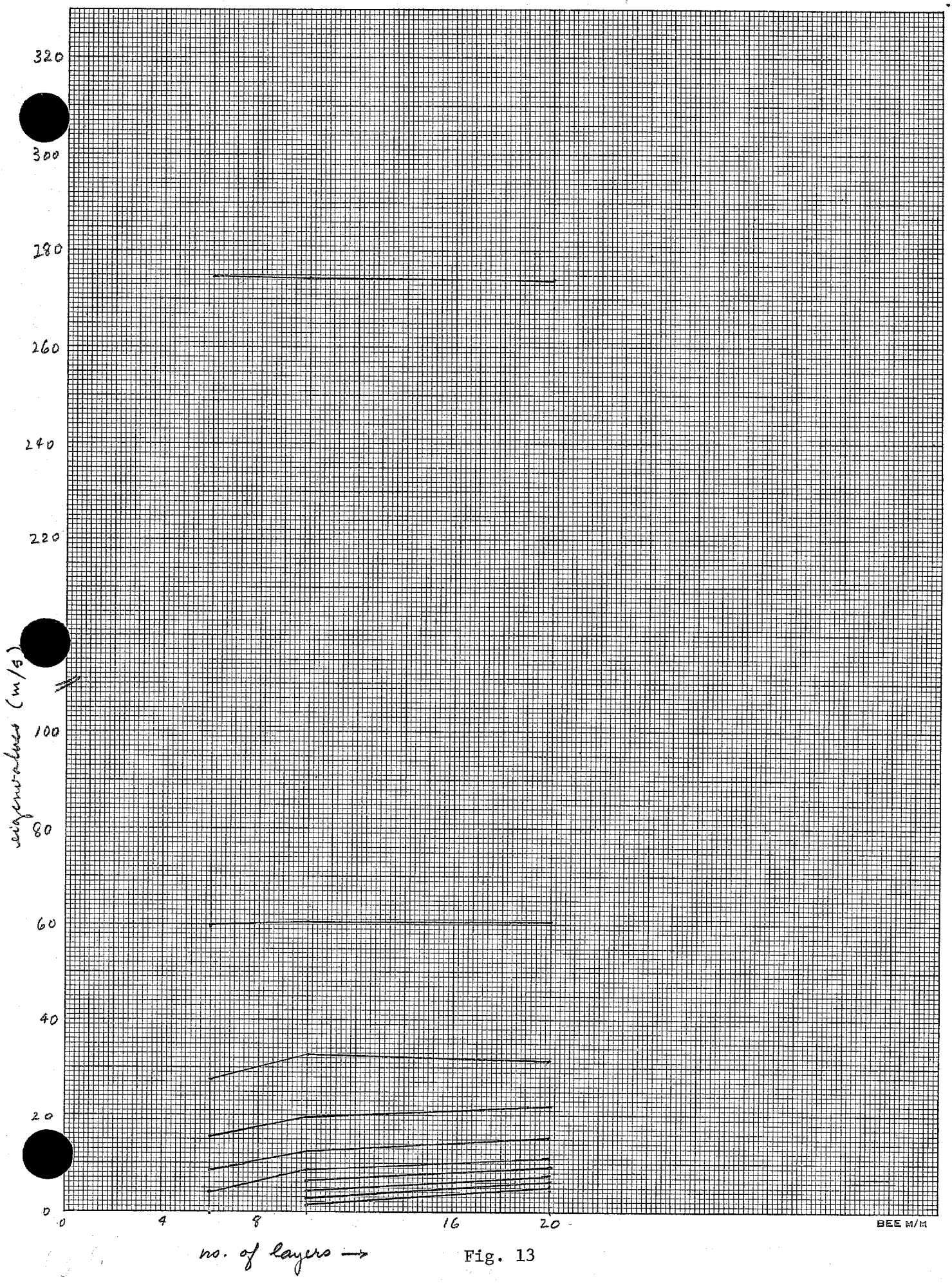
320
300
280
260
240
220
100
80
60
40
20
0
0
4
8
16
20
BEE M/M
no. of layers →

Fig. 13

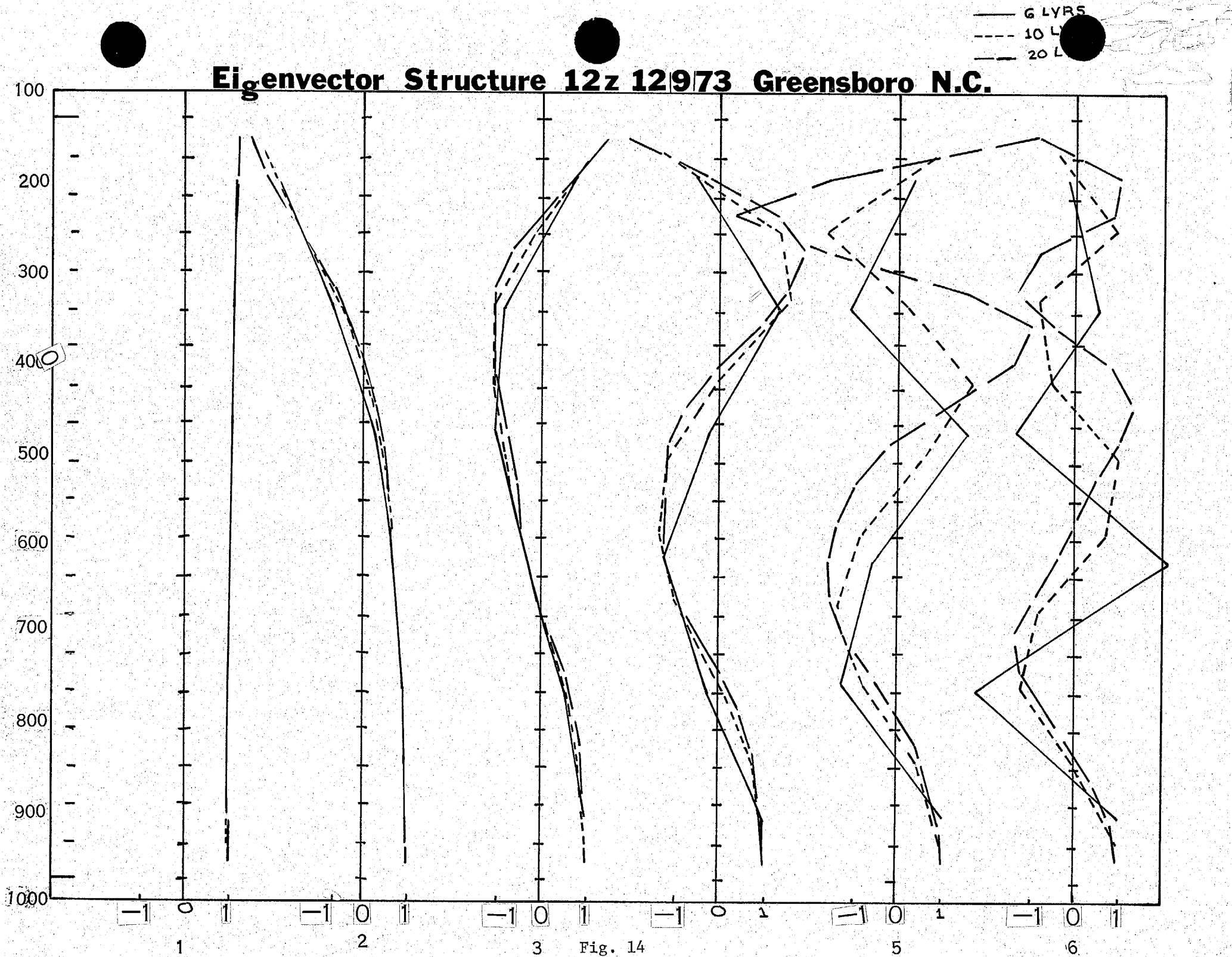
Eigenvector Structure 12z 12/9/73 Greensboro N.C.
6 LYRS
10 L
20 L
100
200
300
400
500
600
700
800
900
1000
-1
0
1
1
2
3
5
6

Fig. 14

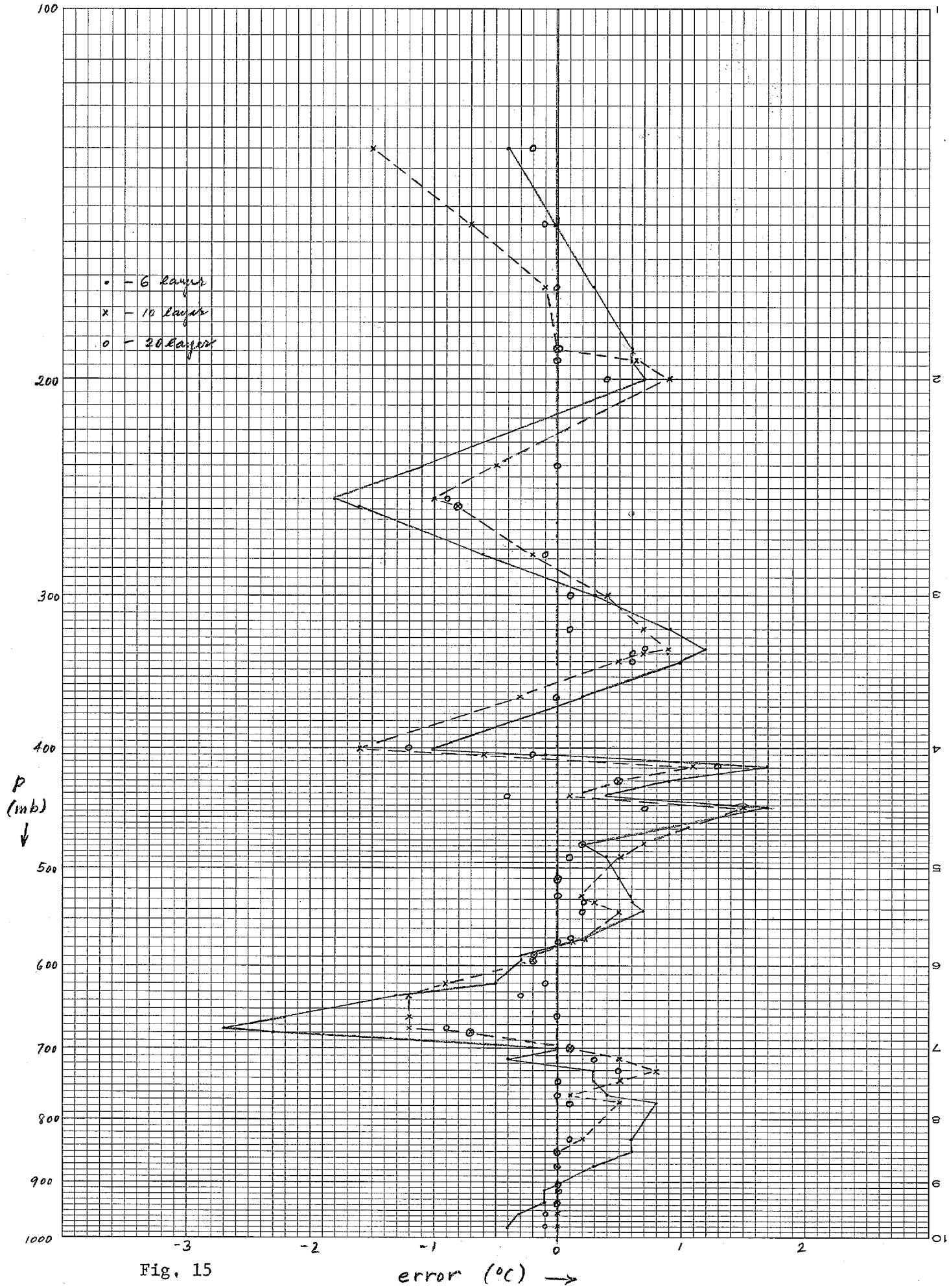

Fig. 15